KAERI/TR-1919/2001

균일 및 비균일 가열 수직환상관에서 임계열유속에 대한 실험 연구

Experimental Study on the CHF in Uniformly and Non-Uniformly Heated Vertical Annuli

한국원자력연구소

KAERI/TR-1919/2001

Experimental Study on the CHF in Uniformly and Non-Uniformly Heated Vertical Annuli

Se-Young Chun, Sang-Ki Moon, Heung-June Chung, Jong-Kuk Park,
Bok-Deuk Kim, Young-Jung Youn, Moon-Ki Chung

September 2001

Thermal-Hydraulic Safety Research Team
Korea Atomic Energy Research Institute
150 Dukjin-dong, Yusong-gu, Taejon, 305-353, Korea

제 출 문

한국원자력연구소장 귀하

본 보고서를 “원전 안전계통 실증실험” 과제에서 수행된 균일 및 비균일 가열 수직환상관에서의 임계열유속에 대한 실험 연구의 기술보고서로 제출합니다.

2001. 9. 20

저 자 : 천세영 (열수력안전연구팀)
문상기 (열수력안전연구팀)
정홍준 (열수력안전연구팀)
박종국 (열수력안전연구팀)
김복득 (열수력안전연구팀)
윤영중 (열수력안전연구팀)
정문기 (열수력안전연구팀)

요 약 문

현재까지 한국원자력연구소에서는 RCS CHF Loop를 이용하여 Zero-Flow 및 저유속 조건에서 균일 및 비균일하게 가열되는 수직 환상관에서 물을 이용한 임계열유속 실험을 수행하였다. 저유속 조건에서 수행된 기존의 임계열유속 실험이 낮은 압력조건에서 주로 수행되었기 때문에, 본 실험에서는 광범위한 압력조건하에서 Zero-Flow 및 저유속 조건에서의 압력이 임계열유속에 미치는 영향을 살펴보았다. 또한 저유속 조건에서 수직방향 열유속분포가 미치는 영향을 고찰하기 위해, 동일한 기하학적 형상을 갖는 균일 및 비균일 가열 수직환상관을 이용하였다. 본 보고서는 이러한 일련의 실험들의 결과를 종합하고, 임계열유속 상관식의 개발 및 코드 개발에 이용될 수 있도록 임계열유속 실험 데이터를 제공하기 위해 작성되었다.

임계열유속 실험은 계통압력 0.54 - 15.15 MPa, 질량유속 0, 200 - 650 kg/m^{2}s, 입구과냉도 75 - 360 kJ/kg 및 출구건도 0.07 - 0.57의 조건에서 수행되었다. 저유속 조건에서는 균일 및 비균일하게 가열되는 수직환상관에서 각각 242개와 290개의 임계열유속 데이터를 생산하였다. 시험관 하부를 폐쇄하여 수행한 Zero-Flow 조건에서의 임계열유속 데이터는 균일 및 비균일 가열 시험관에서 각각 41개와 94개의 데이터가 생산되었다.

임계열유속 실험결과 임계열유속에 미치는 압력, 유량, 입구과냉도 등의 영향은 기존 원형관에서와 비슷하게 나타났다. 낮은 압력에서는 임계열유속의 거동이 복잡하게 나타났다. 또한 낮은 압력조건에서 수직방향 열유속분포가 임계열유속에 미치는 영향이 상대적으로 큰 것으로 나타났다. 본 보고서에서는 실험 데이터의 정리를 목적으로, 단순한 변수 경향 등에 대해서만 논의하기로 한다. 유동양식의 고찰, 기존 상관식과의 비교, 새로운 상관식의 제안 등 기타 결과는 참고문헌에 자세히 나타나 있으므로, 본 보고서에서는 생략한다.

SUMMARY

Up to now, KAERI has performed critical heat flux experiments in water under zero-flow and low-flow conditions using a RCS CHF loop facility with uniformly and non-uniformly heated vertical annuli. Since the existing CHF experiments were mainly performed under low-pressure conditions, we performed the CHF experiment to investigate the pressure effect on the CHF under zero-flow and low-flow conditions for a wide range of system pressures. Also, two vertical annuli with the same geometry have been used to investigate the axial heat flux distributions on the CHF. This report summarizes the experimental results and provide the CHF data that can be used for the development for CHF correlation and a thermal hydraulic analysis code.

The CHF data have been collected for system pressures ranging from 0.57 to 15.15 MPa, mass flux 0 and from 200 to 650 kg/m^{2}s, inlet subcooling from 75 to 360 kJ/kg and exit quality from 0.07 to 0.57. At low-flow conditions, the total number of data are 242 and 290 with uniformly heated- and non-uniformly heated test sections, respectively. 41 and 94 CHF data are generated with uniformly heated- and non-uniformly heated test sections, respectively, in zero-flow CHF experiments that are performed by blocking test section bottoms.

The CHF experiment result shows that the effects of system pressure, mass flux and inlet subcooling are consistent with conventional understandings and similar to those for round tubes. The behavior of the CHF is relatively complex at low pressures. Also, the effects of axial heat flux profiles are large at low-pressure conditions. Because the main objective of this report is to summarize the experimental data, we discuss the parametric trends only. Other analysis results such as CHF flow pattern, mechanism, comparison with conventional correlation and development of new correlation can be found in references that the present authors have written.

TABLE OF CONTENTS

List of Tables

List of Figures

Nomenclature

D_{hy} Hydraulic diameter

D_i Inner diameter of annulus test section

D_o Outer diameter of annulus test section

G Mass flux

g Gravitational acceleration

L_B Boiling length in the heated section

L_h heated length

P System pressure

Q_c Total power from inlet to CHF location (critical power)

q_c Average heat flux (CHF) from inlet to CHF location

$q_{C,B}$ Average CHF over the boiling length

X Thermodynamic quality

X_c Thermodynamic quality at CHF location (critical quality)

Z Distance from the bottom end of the heated section

Greeks

α Average void fraction from the bottom end of the heated section to location Z

α_o Average void fraction for the saturated condition at the bottom end of the heated section

Δh_i Inlet subcooling

ΔP Differential pressure

ΔT_{sub} Subcooling temperature at the bottom end of the heated section

ρ Density

Subscripts

c CHF location or critical

g Vapor

l Liquid

NU	Non-uniform
sat	Saturated
sub	Subcooled
UN	Uniform

I. Introduction

In the boiling heat transfer system, it has been observed experimentally that, above a certain heat flux, the liquid can no longer permanently wet the heater surface. This situation leads to an inordinate decrease in the surface heat transfer. This heat flux is commonly referred to as the critical heat flux (CHF). The CHF in nuclear reactors is one of the important thermal hydraulic parameters limiting the available power, because the inordinate rise of reactor fuel surface temperature under CHF conditions is sometimes sufficient to cause the melting of the fuel materials.

Presently, many aspects of CHF phenomena are well understood and several reliable prediction methods are available for most of the operating conditions of nuclear reactors. Most of the CHF studies have been concentrated on high pressure and high flow rate conditions corresponding to normal operation ranges of light water reactors (LWRs). Therefore, though several prediction methods for CHF that are reliable for normal operating conditions of LWRs have been developed, these prediction methods have a relatively narrow range of validity.

However, the CHF behavior in low flow conditions is not well identified, which is of importance in the safety of nuclear reactors during operational transients and accidents such as LOCA (Loss-Of-Coolant Accident) or a steam line break accident without offsite power in LWRs. Furthermore, the CHF under low flow conditions plays an important role in thermal hydraulic behavior for accident analyses of LWR, research reactors, and advanced nuclear reactors. Therefore, in order to achieve optimal design and to ensure a high degree of safety of future LWRs, the CHF characteristics under low flow conditions must be clearly understood. However, most of the experimental studies for CHF under low flow conditions have been performed under near atmospheric pressure conditions.

Many experiments have been performed on CHF in tubes or annuli, and a large array of CHF correlations has been available. The significance of annular geometry experiments lies in the fact that the flow structure around rods in

the rod bundle is of annular type and, moreover, the peripheral subchannel of rod bundle may be assimilated to a part of an annulus having an inside heated rod and unheated shroud. However, available CHF data for annuli under low flow conditions are much more limited than tube CHF data. In practice, the AECL-UO look-up table (Groeneveld et al., 1986) and Biasi correlation (1967) being used in the thermal hydraulic system analysis codes such as RELAP5/MOD3 (Weaver et al., 1991) and TRAC-PF1 (Liles et al., 1984) are based on an extensive data base of CHF values obtained in round tubes. For annular channels, there are available CHF data from the experiments of Janssen and Kervinen (1963), Becker et al. (1965) and Barnett (1966). Janssen and Kervinen performed CHF experiments for the internally heated vertical annulus channel in the pressure range of 4.1 - 10 MPa and mass flux range of 175 - 8400 kg/m^2s. Becker et al. obtained CHF data for annuli with an inside heater rod in the pressure range of 1.0 - 3.5 MPa and mass flux range of 50 - 650 kg/m^2s. Barnett compiled CHF data for uniformly heated annuli at a pressure of 6.9 MPa and mass fluxes from 190 to 8400 kg/m^2s. In recent years, Mishima and Ishii (1982), Rogers et al. (1982), El-Genk et al. (1988), Schoesse et al. (1997) and Park et al. (1997) performed CHF experiments with more attention on very low flow (several ten kg/m^2s) in an internally heated annulus. Their studies were conducted in test sections with heating lengths below 1.0 m near atmospheric pressure conditions. Also, Kumamaru et al. (1990) investigated the CHF in an internally heated annulus having a heating length of 2.0 m under a medium pressure of 3 MPa, low mass fluxes of 105 - 320 kg/m^2s and mixed inlet conditions, that is, conditions in which a two phase mixture of water and steam enters the test section. The CHF data presented in the above references did not cover a wide range of pressure conditions, and only a few experiments were performed in a low flow region under medium and high pressure conditions. Consideration for the influence of pressure on CHF at low flow conditions has not been given carefully until now.

Since 1991, KAERI has performed CHF experiments using vertical annuli under low-flow and a wide range of pressure conditions. Two kinds of

annulus test sections have been used to investigate the effect of axial heat flux distributions on the CHF. The first one has uniform axial heat flux distributions and the other one has symmetric cosine axial heat flux distributions. This report presents the results from the CHF experiments carried out in internally heated annuli at low flow with a wide range of pressure conditions. Also, this report presents the results from zero-flow CHF experiments that were performed by blocking inlet flow.

II. Test Facility and Test Sections

Test Facility

The CHF experiments reported in this paper have been conducted in the Reactor Coolant System thermal hydraulics loop facility (RCS loop facility) of the Korea Atomic Energy Research Institute (KAERI). The principal operating conditions of the RCS loop facility are

operating pressure	: 0.5 - 16 MPa
test section flow rate	: 0.03 - 3 kg/s
maximum water temperature	: 347 ^{o}C
available heating power of test section	: 500 kW.

Figure II-1 shows the flow diagram of the RCS loop facility. It basically consists of a main circulating pump, preheater, CHF test section, steam/water separator, pressurizer and cooler. Stainless steel, SUS 304, was used as construction material for the loop facility to prevent corrosion. The loop is filled with de-ionized water. The flow rate of the test section inlet is controlled by the adjustments of the motor speed of the circulating pump and the flow control valve. Three kinds of orifice flow meters with different measuring ranges are installed to measure the flow rate of water entering the test section. A throttling valve located up stream of the test section inlet is used to avoid the flow fluctuations, which are usually observed under low flow conditions. The preheater with a power of 40 kW adjusts the degree of the subcooling of water entering the test section. The steam generated in the test section is condensed through the condenser attached in the steam/water separator. The system pressure is maintained using the pressurizer with an immersion heater with a power of 40 kW.

Test Section for Uniform Axial Heat Flux Profile

Figure II-2 shows the details of the test section used in this experimental study. The test section, which is an internally heated annulus flow channel, consists of an outer pipe with a 19.4 mm inside diameter and an inner heater rod with a 9.54 mm outer diameter having a heated length of 1842 mm at

room temperature. The inner heater rod is heated indirectly by electricity with uniform axial power distribution. The sheath and heating element of the heater rod are made of Inconel 600 and Nichrome, respectively. For measuring the heater rod surface temperatures and detecting CHF occurrence, six Chromel-Alumel thermocouples with sheath outer diameters of 0.5 mm are embedded on the outer surface of the heater rod. The temperature sensing points of these thermocouples are located at 10, 30, 110, 310, 510 and 910 mm from the top end of the heated section.

Test Section for Non-Uniform Axial Heat Flux Profile

The annulus test section for the non-uniform axial heat flux profile has similar geometry to the one for uniform axial heat flux profile. As shown in Fig. II-3, the annulus test section consists of an outer pipe with a 19.4 mm inside diameter and an inner heater rod with a 9.53 mm outer diameter. The inner heater rod is heated indirectly by AC power. Six K-type thermocouples with sheath diameters of 0.5 mm are embedded on the surface of the heater rod to measure the heater rod surface temperatures and detect CHF occurrence. The inner rod having a heated length of 1843 mm is uniformly divided into 10 steps to simulate a symmetric chopped cosine axial heat flux profile, as shown in Fig. II-4. The figure also shows the thermocouple locations and the approximate axial heat flux profile. The temperature sensing points of these thermocouples are located at 10, 20, 301, 400, 510 and 740 mm from the top end of the heated section. The temperature sensing locations are different from the test section with a uniform axial heat flux profile, because the CHF for a non-uniform axial heat flux profile usually occurs at the upstream location of the exit of the test section rather than the exit itself.

Measurement System and Uncertainties

The main parameters measured in this experiment are the water temperatures at the bottom and top of the heated section, the surface temperatures of the heater rod, the pressures at the inlet and outlet plenums, the differential pressures in the test section, the flow rate of the test section

inlet and the power applied to the heater rod.

All the electrical signals from the sensors and transmitters are processed and analyzed by a data acquisition and control system consisting of A/D and D/A converters, and a workstation computer. The data acquisition system consists of the high speed scanning A/D converter (HP E1413), computer processor (HP V743 controller), D/A converter (HP E1328) and hard disk. The high speed scanning A/D converter converts the analog signal from various instruments to a digital signal. The A/D converter collects the signals in 100 kHz with 16 bit of accuracy. HP V743 controller collects the digital signal, processes and stores the instrument signals. The data acquisition and control system measures various experimental data in real time, and controls the main heater power at CHF occurrence. Various electrical signals (voltage and current) from instrument feed into the controller through the VXI bus. These signals are finally displayed to the monitor by the HP-VEE program after calculation using data processing software. Fig. II-5 shows the structure of the data acquisition and control system. Table II-1 shows the detailed specification of the data acquisition and control system.

Computer programs are prepared to control the data acquisition system, to collect the measured signals such as voltage and current, and to convert the measured signals into physical parameters such as temperature, pressure, differential pressure, flow rate, and heater power. These programs are made by HP-VEE, C-SCPI and C language. The C language has a steam table to convert the electrical signal into physical parameters and controls the sampling time and the number of sampling. The sampling time is 20 msec and the final physical data are stored for 60 sec before CHF occurrence. Fig. II-6 shows the display result of the HP VEE main program.

The uncertainties of the measuring system were estimated from the calibration of sensors and the accuracy of equipment, according to the ANSI/ASME PTC 19.1 code (1985). The evaluated maximum uncertainties of pressures, flow rates and temperatures were less than $\pm$0.3 %, $\pm$1.5 % and $\pm$0.6 % of the readings in the range of interest, respectively. The uncertainty of the heat flux calculated from the applied power was always less than $\pm$1.0

% of the readings. Before starting a set of experiments, the pretests (i.e., the heat balance tests) were carried out to estimate the heat loss in the test section, so the heat loss was included in the value of actual heat flux.

Test Procedure

The CHF experiments are performed by the following procedures. After setting the water flow rate, inlet subcooling and pressure at the desired values, the electric power to the test section is increased gradually in small steps. At each power level, the measured parameters are allowed to stabilize before raising the power level again. This process continues until CHF occurs. In the experiments, CHF is determined when the temperature of the heater surface increases sharply and is 100 K higher than the saturation temperature. When the CHF occurs, the heater power is automatically decreased to 80 % or tripped using a CHF detector.

Table II-1. Test section geometry

Parameter	Uniformly heated test section	Non-uniformly heated test section
Annulus inner diameter, mm	9.54	9.53
Annulus outer diameter, mm	19.4	19.4
Heated length, mm	1842	1843
Hydraulic diameter, mm	9.86	9.87
Heated equivalent diameter, mm	29.91	29.96
Axial heat flux distribution	uniform	symmetric chopped cosine
No. of thermocouple	6	6
Distance of thermocouple below top of heated length, mm	10, 30, 110, 310, 510, 910	10, 20, 301, 400, 510, 740

Table II-2. Specifications of data acquisition and control system

Model	Description	Technical Specification
E1401A	VXI C-size Mainframe	- 13 Slots, 650 W
E1498A	VXI Embedded Controller (V743/100)	- Processor : PA-RISC 7100LC - RAM 128 MB, 100 MHz
C3023T	SCSI Mass Storage	- HDD 2 GB, DDS 1.3GB
E1413A	Scanning A/D Converter (64 Channel x 2 EA)	- 16 bit, 100 kHz - Direct voltage input : 64 channel - Max. input voltage : +16V peak - Input impedance : > 100 MOhm
E1328A	D/A Converter (4 Channel)	- 12 bit, 20 msa/s
A1079C	Color Monitor	- 19" (1280 x 1024 resolution)
C1208A	Laser Printer	- Model : HP 4MV Laserjet Printer
S/W	1) HP-UX (Rev. 9.0) 2) VEE-Test (Rev. 2.0) 3) C-SCPI (S700)	

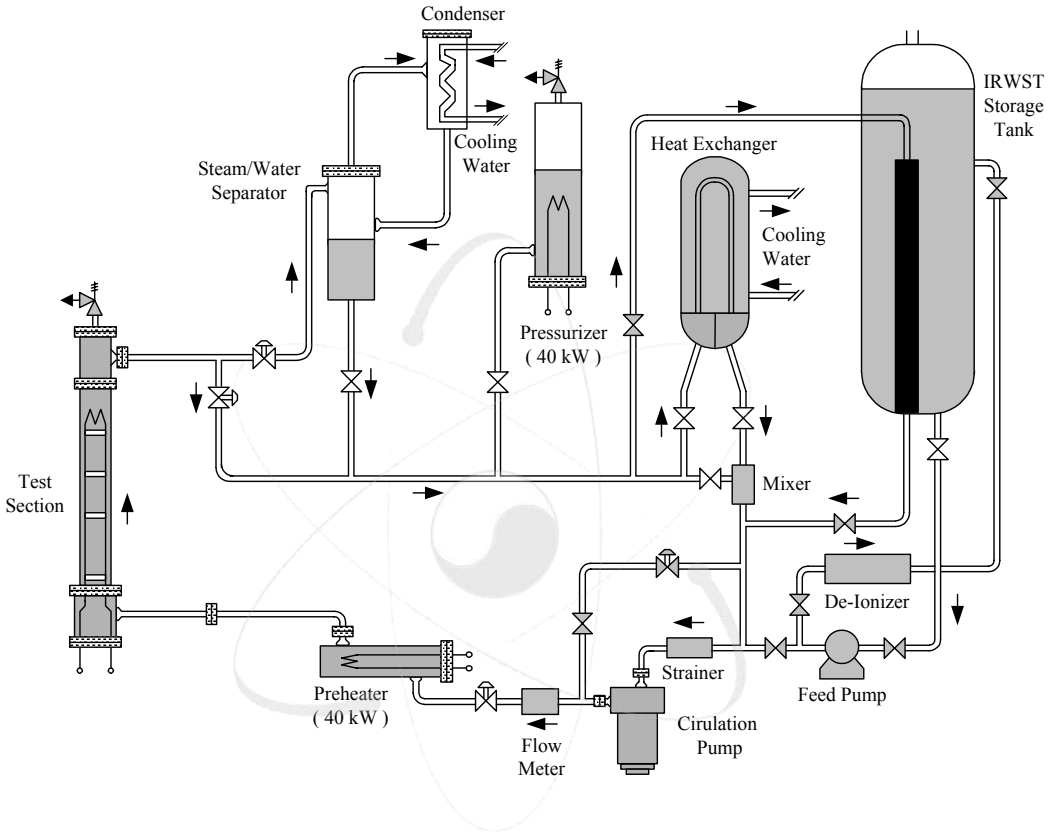

Fig. II-1. KAERI RCS loop schematics

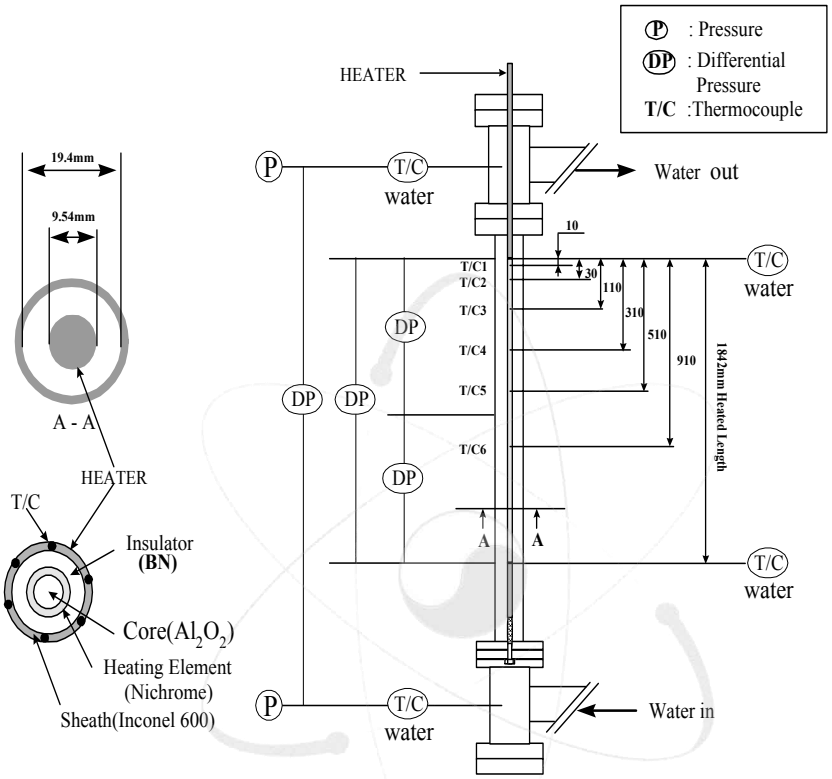

Fig. II-2. Test section for uniform axial heat flux profile

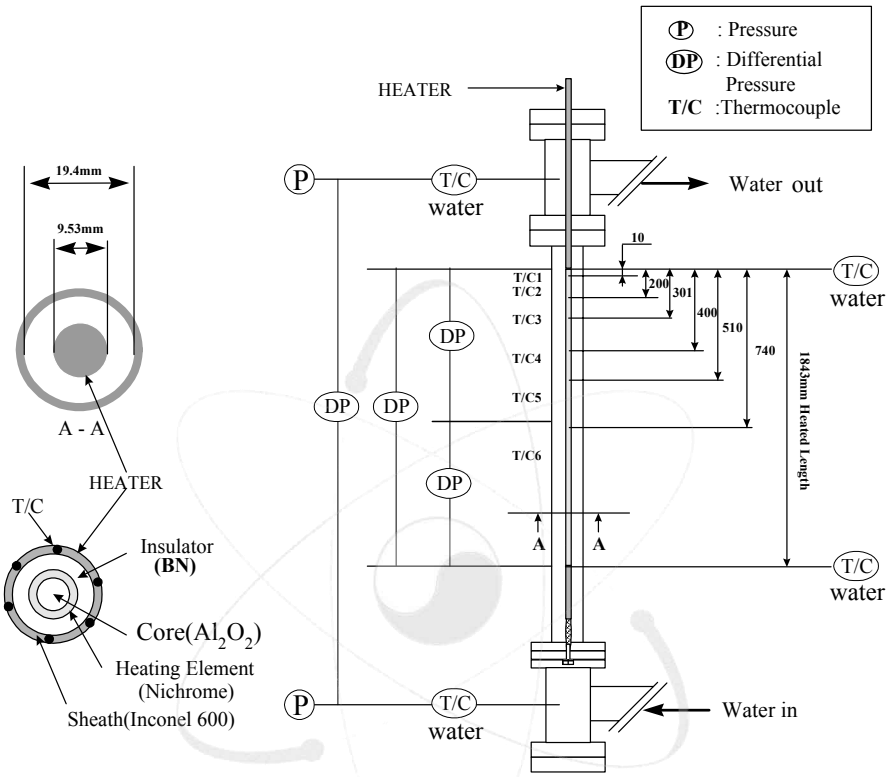

Fig. II-3. Test section for non-uniform axial heat flux profile

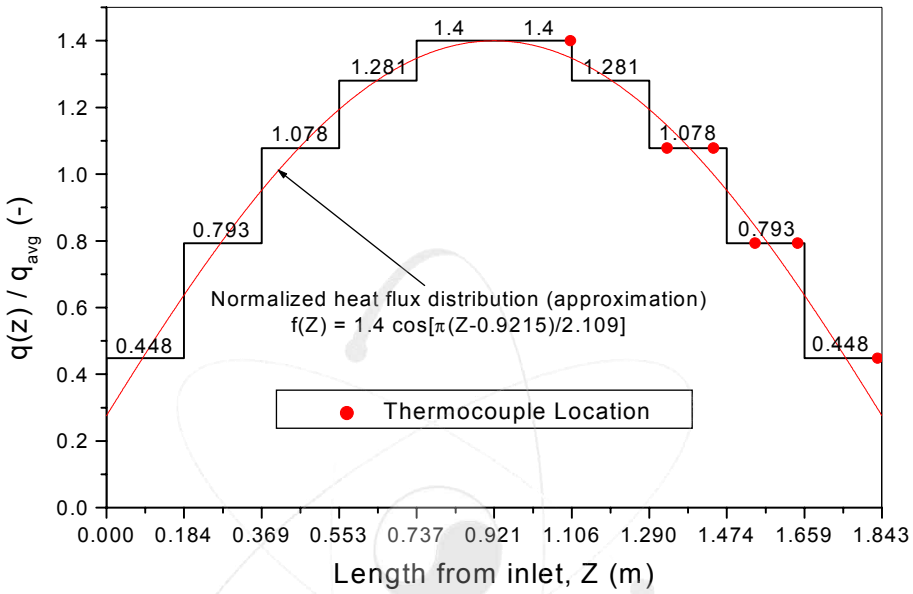

Fig. II-4. Axial heat flux profile of the test section

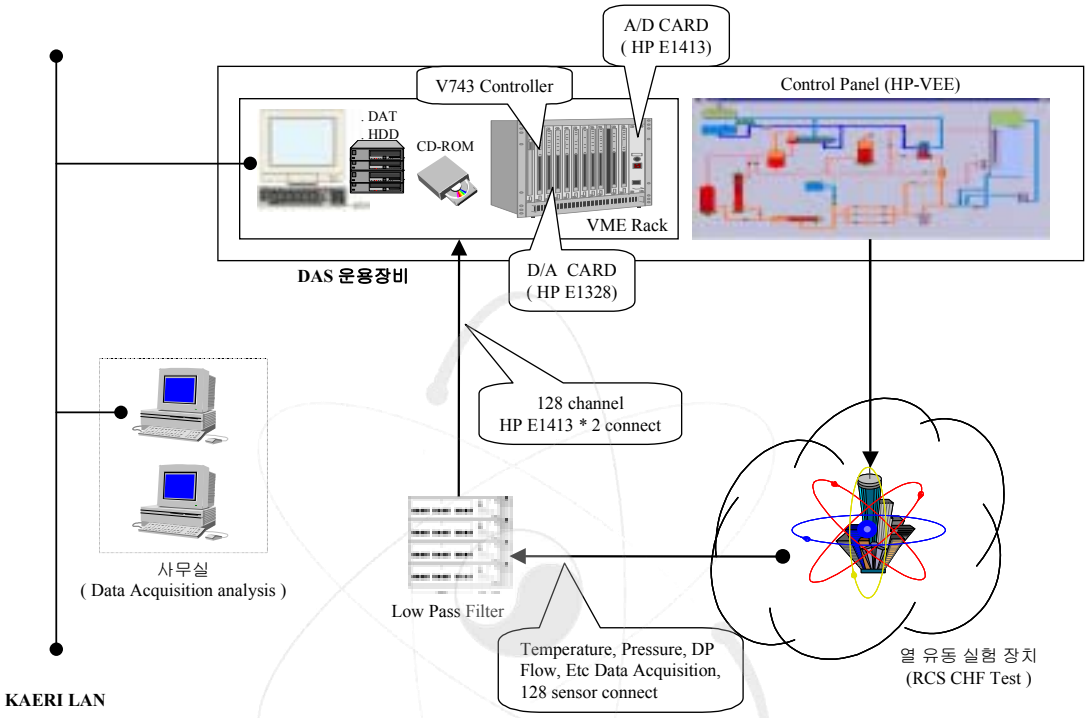

Fig. II-5. Schematic diagram of data acquisition and control system

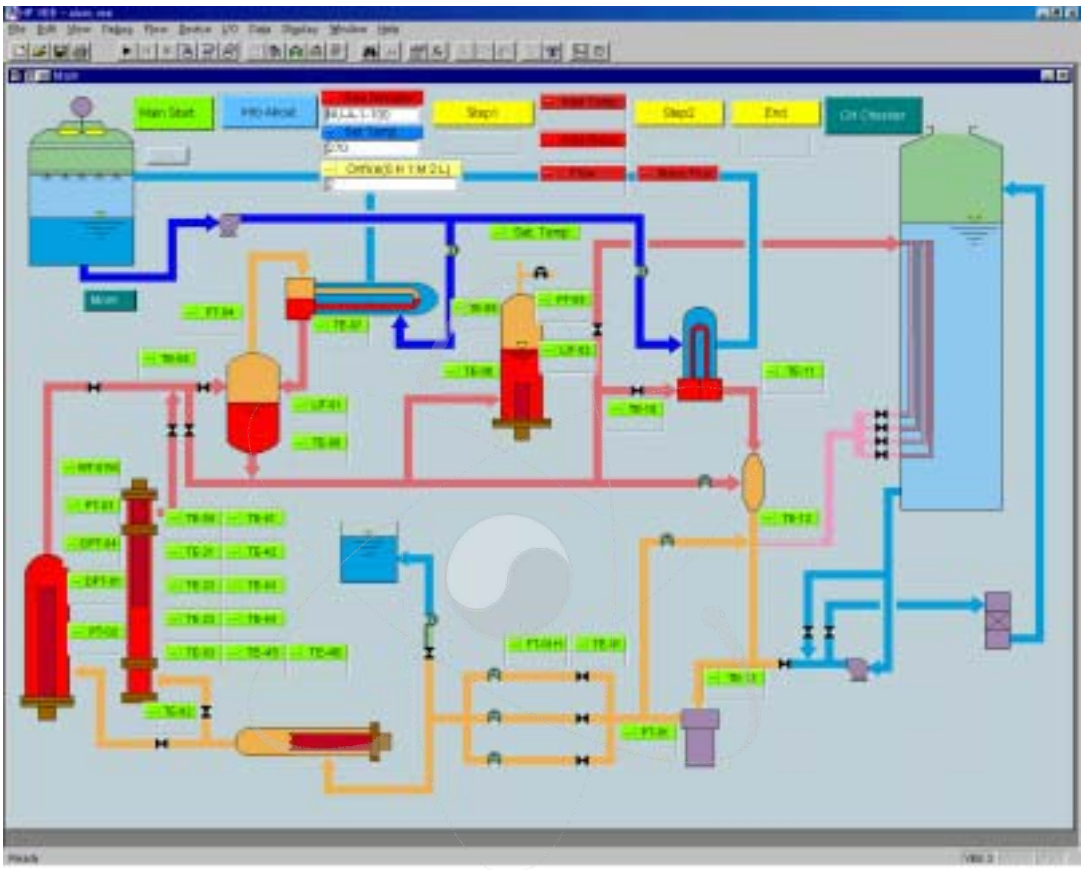

Fig. II-6. Display results of HP-VEE main program

III. CHF Experiment Using Uniformly Heated Vertical Annulus

Using the test section with a uniform axial heat flux, a total of 240 CHF data have been collected for water inlet subcooling ranging from 76 to 360 kJ/kg, mass fluxes from 200 to 650 kg/m^{2}s, system pressure from 0.54 MPa to 15.15 MPa, and exit quality from 0.11 to 0.54. Appendix B shows the CHF data base for the test section with the uniform heat flux profile.

Parametric Trends

The CHF with a uniform axial heat flux profile occurs at the exit of the test section. Therefore, in this section, the critical means the conditions at the exit itself.

The CHF increases with an increasing mass flux, as shown in Figs. III-1 ~ III-3. The critical quality decreases with an increasing mass flux, as shown in Figs. III-4 ~ III-6. This trend is more prominent as the pressure is higher and the mass flux is lower. Figs. III-7 ~ III-9 show the inlet subcooling effect on the CHF for various system pressures. The inlet subcooling effect on CHF is not as clear at a low pressure. As the pressure increases, however, the figures show a linear relationship between the inlet subcooling and the CHF.

As shown in Figs. III-10 ~ III-12, the average CHF increases sharply with pressure in high flow conditions, and reaches local maximum values at about 2 ~ 4 MPa.

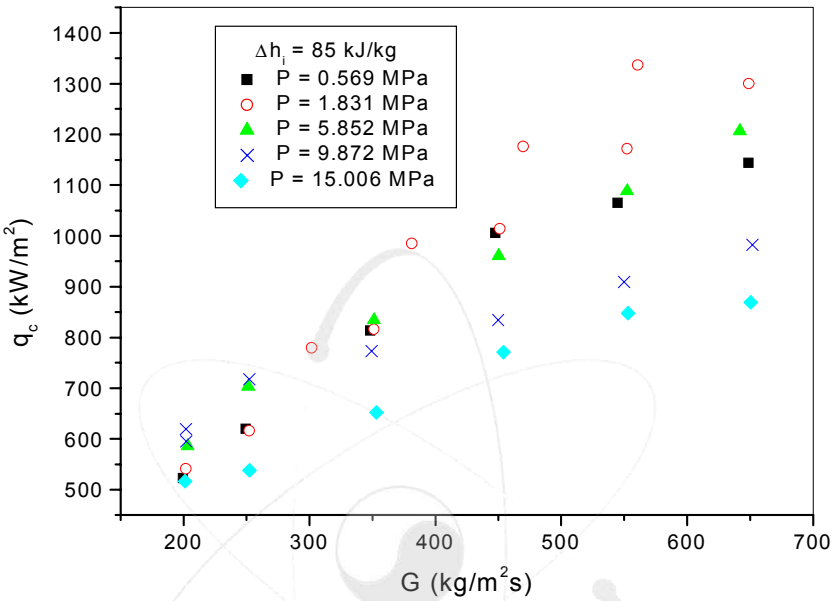

Fig. III-1. Effect of mass flux on the CHF (Δh_i = 85 kJ/kg)

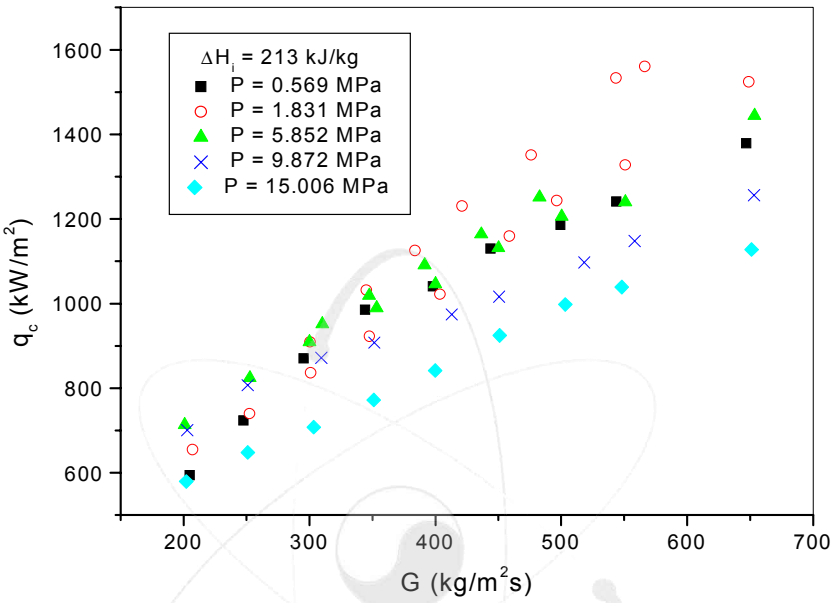

Fig. III-2. Effect of mass flux on the CHF (Δh_i = 213 kJ/kg)

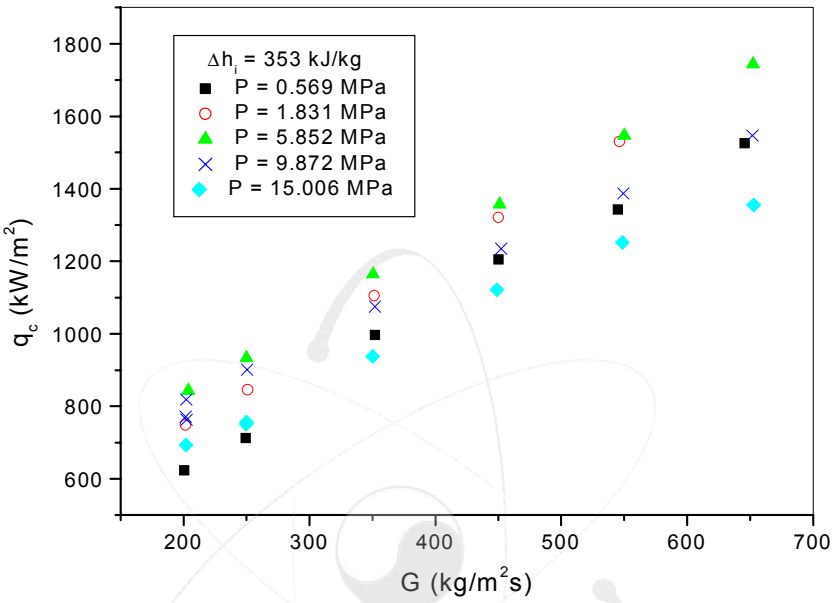

Fig. III-3. Effect of mass flux on the CHF (Δh_i = 353 kJ/kg)

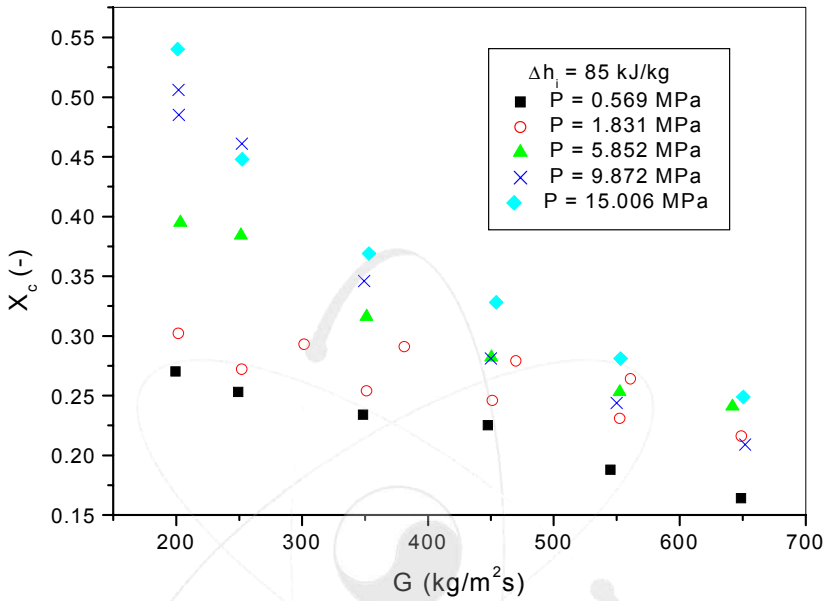

Fig. III-4. Effect of mass flux on the critical quality (Δh_i = 85 kJ/kg)

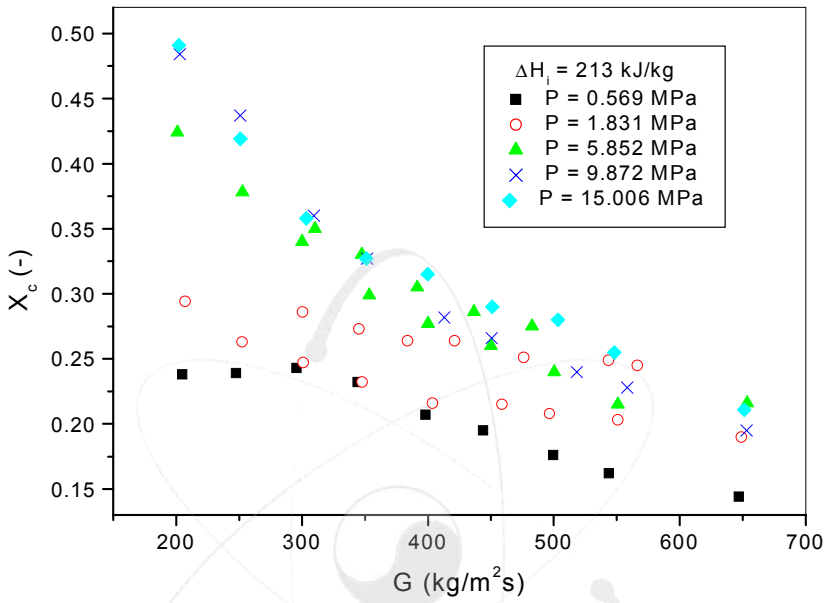

Fig. III-5. Effect of mass flux on the critical quality (Δh_i = 213 kJ/kg)

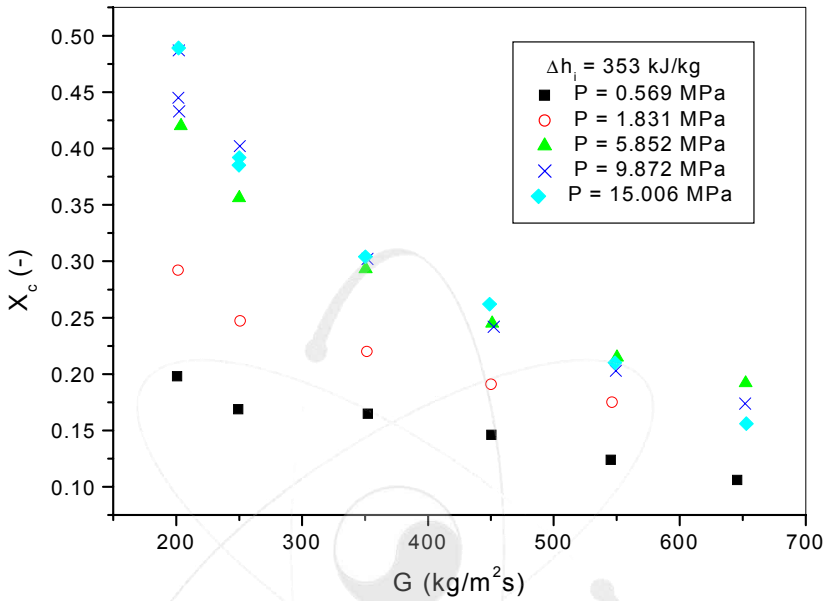

Fig. III-6. Effect of mass flux on the critical quality (Δh_i = 353 kJ/kg)

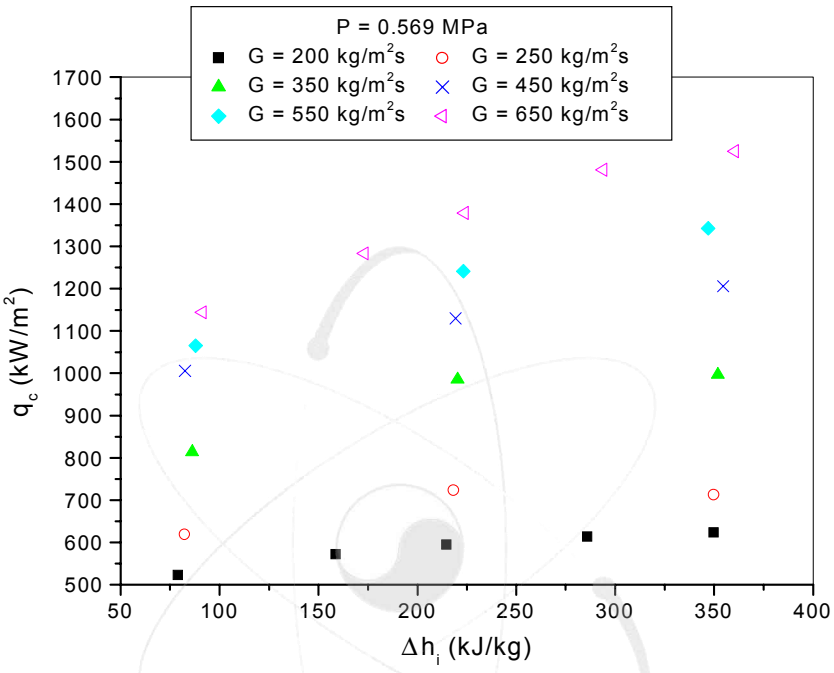

Fig. III-7. Effect of inlet subcooling (0.569 MPa)

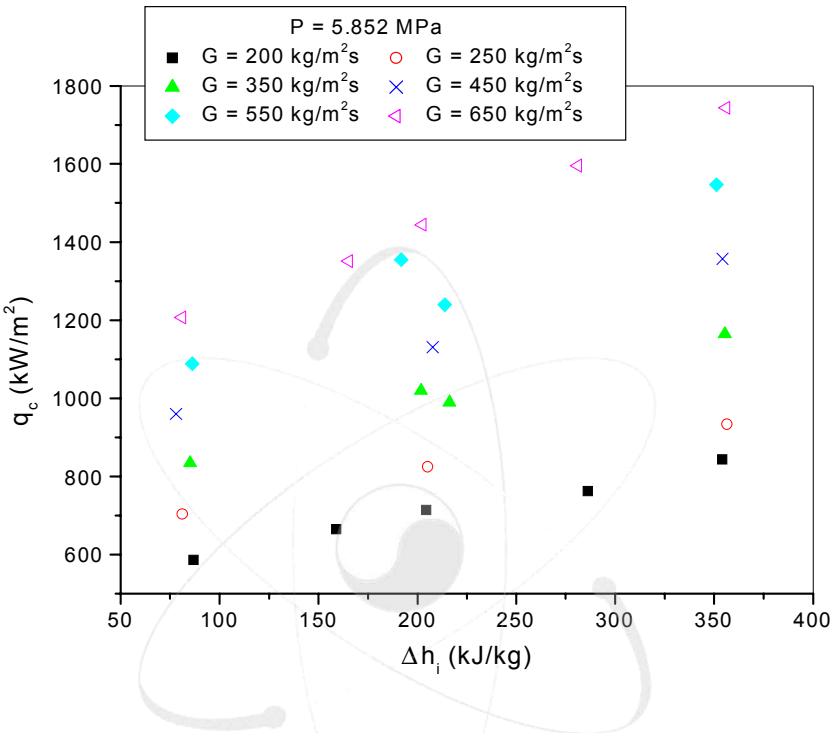

Fig. III-8. Effect of inlet subcooling (5.852 MPa)

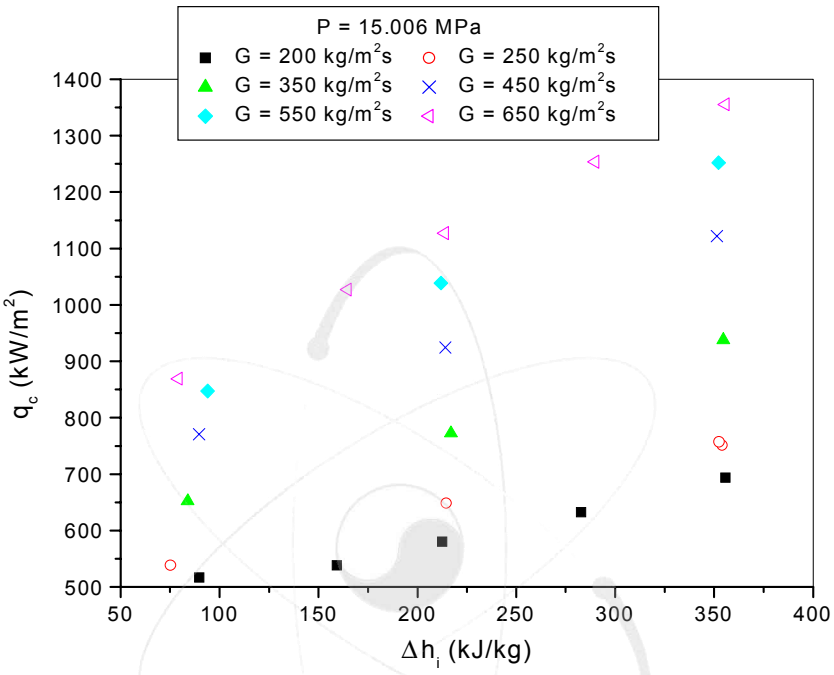

Fig. III-9. Effect of inlet subcooling (15.006 MPa)

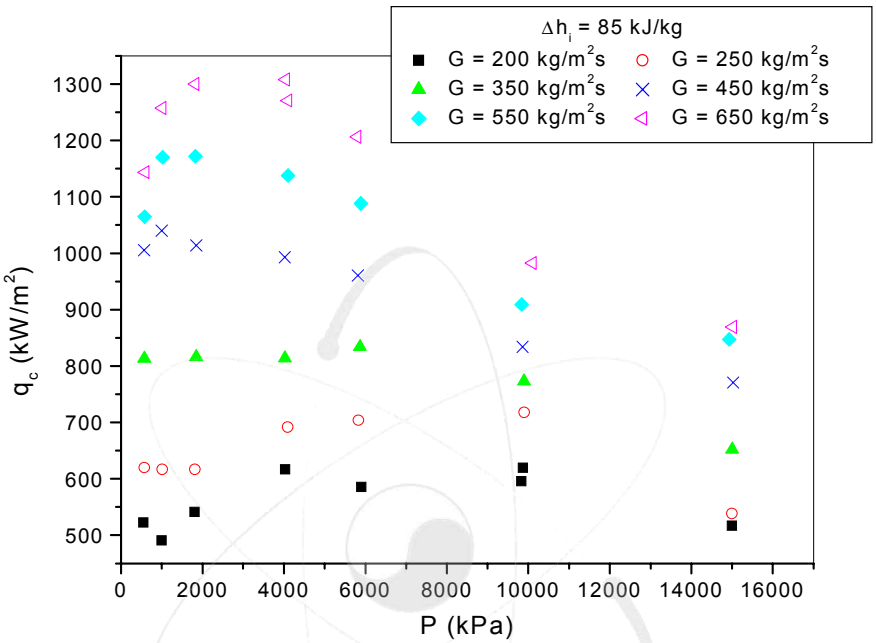

Fig. III-10. Effect of system pressure on the CHF (Δh_i = 85 kJ/kg)

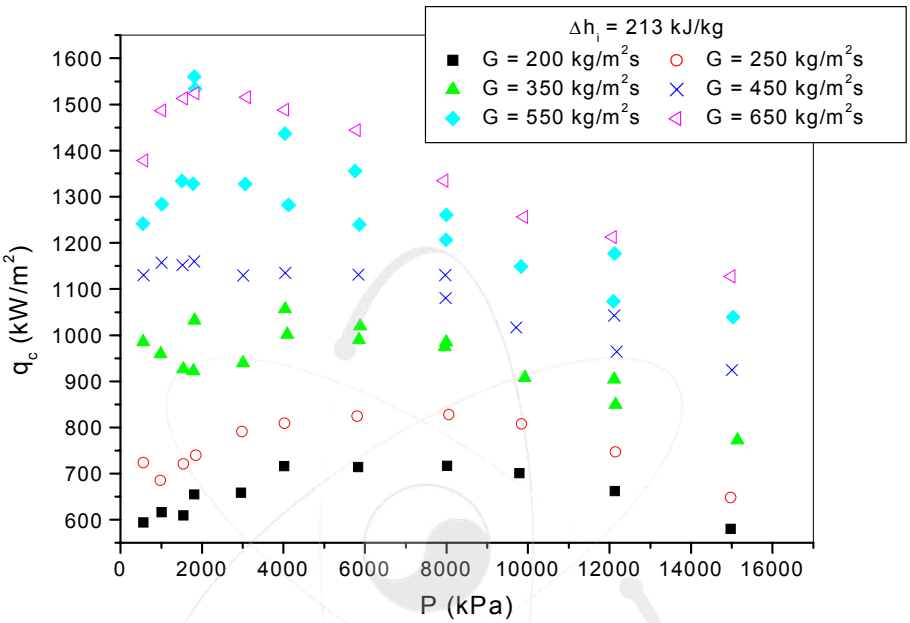

Fig. III-11. Effect of system pressure on the CHF (Δh_i = 213 kJ/kg)

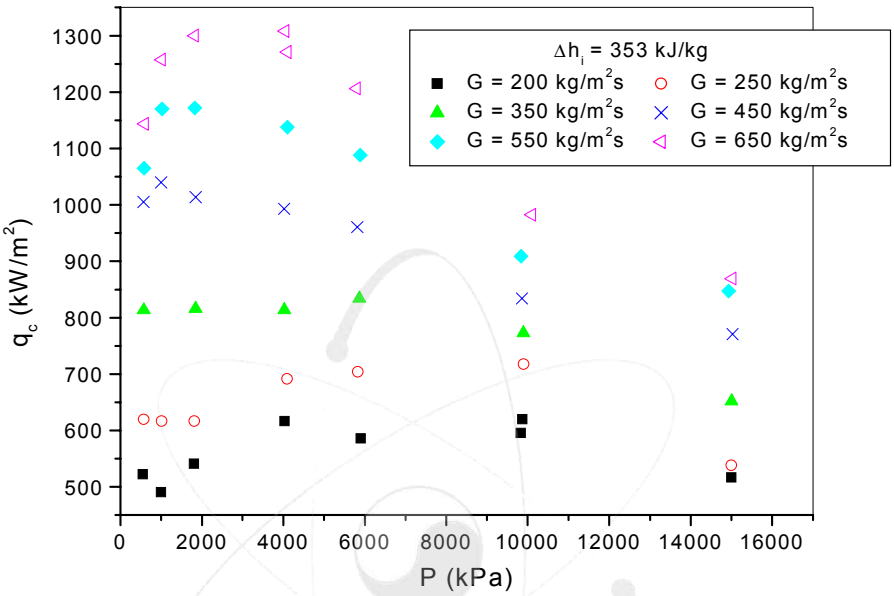

Fig. III-12. Effect of system pressure on the CHF (Δh_i = 353 kJ/kg)

IV. CHF Experiment Using Non-Uniformly Heated Vertical Annulus

Using the test section with a non-uniform axial heat flux, a total of 290 CHF data have been collected for water inlet subcooling ranging from 86 to 353 kJ/kg, mass fluxes from 200 to 650 kg/m^{2}s, system pressure from 0.54 MPa to 15.12 MPa, and exit quality from 0.07 to 0.57. Appendix A shows the CHF data base for the test section with the non-uniform heat flux profile.

For the test section having a non-uniform heat flux distribution, CHF occurs in the upper region of the test section near the exit. In those cases, we should use the local condition parameters at the CHF occurrence point rather than the exit of the test section to properly analyze the CHF data. Since these local parameters are strongly dependent on the upstream conditions and the CHFs are usually regarded as having an upstream effect, especially in the liquid film dryout mechanism, we analyzed the experimental data using the total power (critical power) and average heat flux up to the CHF location, and the critical quality at the CHF location. In the experiments, most of the CHFs occurred at thermocouple 2 or 3, which are located at the upstream location near the exit.

Parametric Trends

The average CHF increases with an increasing mass flux, as shown in Fig. IV-1 ~ IV-3. The critical quality decreases with an increasing mass flux, as shown in Fig. IV-4 ~ IV-6. This trend is more prominent as the pressure is higher and the mass flux is lower. Figures IV-7 ~ IV-9 show the inlet subcooling effect on the average CHF for various system pressures. The inlet subcooling effect on the CHF is not as clear at a low pressure. As the pressure increases, however, the figures show a linear relationship between the inlet subcooling and the average CHF.

As shown in Figs. IV-10 ~ IV-12, the average CHF increases sharply with pressure in high flow conditions, and reaches local maximum values at about

2 ~ 4 MPa.

Effect of Axial Heat Flux Distribution

The CHF data are compared with the CHF data with a uniform heat flux profile. Figures IV-13 ~ IV-15 show the critical power ratio between uniform heat flux CHF data and non-uniform heat flux CHF data. As shown in the figure, most of the critical powers for the non-uniform heat flux are smaller than those for the uniform heat flux profile at fixed inlet conditions. The CHFs for non-uniform axial heat flux distributions are lower up to about 40 % than those for uniform heat flux distributions, with the deviations decreasing with increasing pressure. In particular, the effect of the heat flux distribution is large at low-pressure conditions. As the pressure increases, the effect of the heat flux distribution becomes small. As shown in Fig. IV-16 ~ IV-18, the CHFs for the non-uniform heat flux occur at lower critical qualities than those for the uniform heat flux.

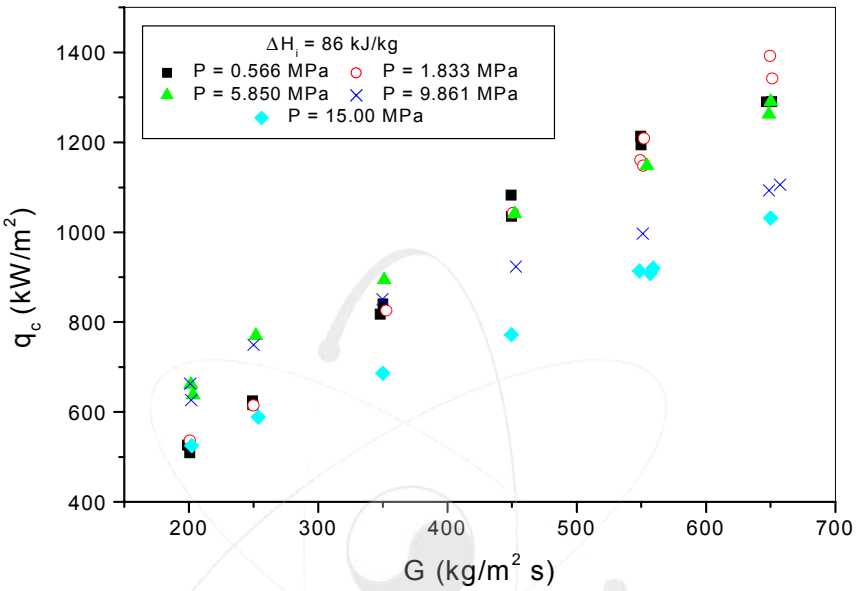

Fig. IV-1. Effect of mass flux on the CHF (Δh_i = 86 kJ/kg)

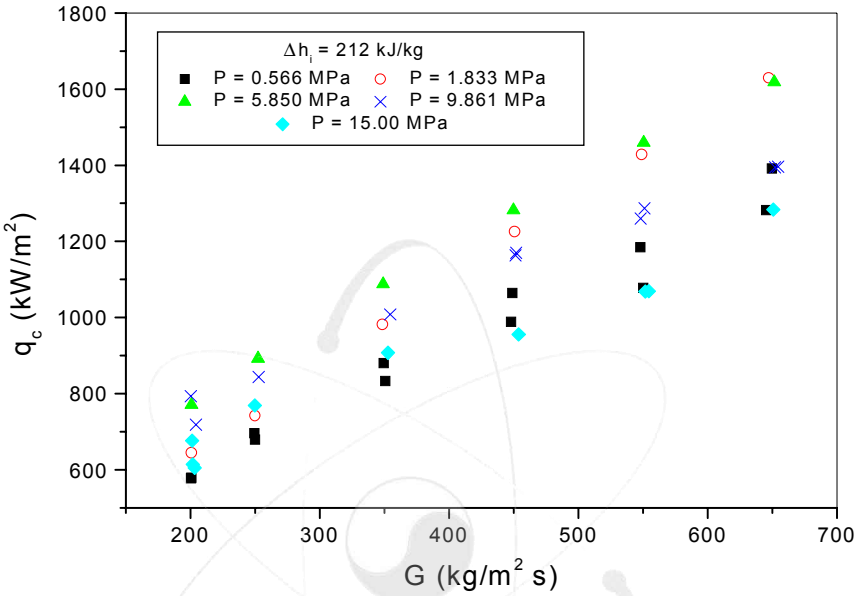

Fig. IV-2. Effect of mass flux on the CHF (Δh_i = 212 kJ/kg)

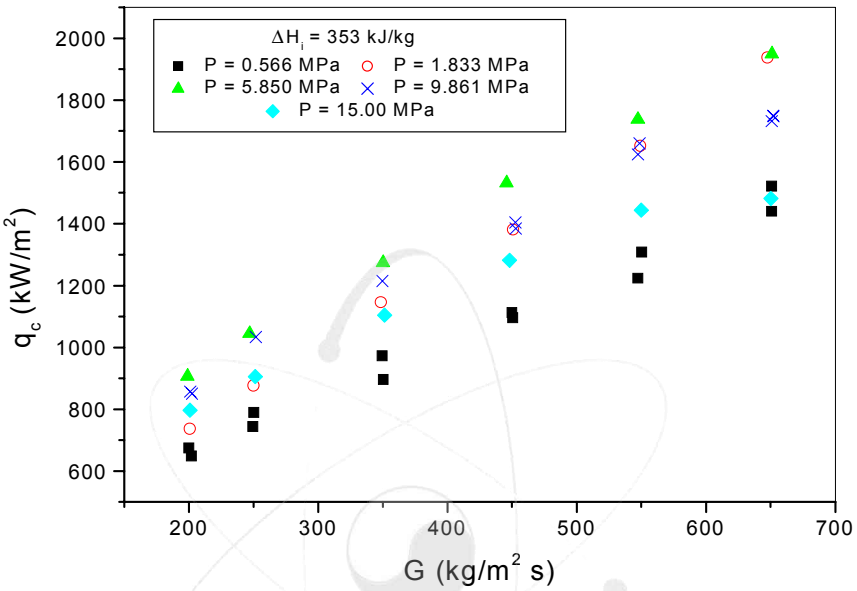

Fig. IV-3. Effect of mass flux on the CHF (Δh_i = 353 kJ/kg)

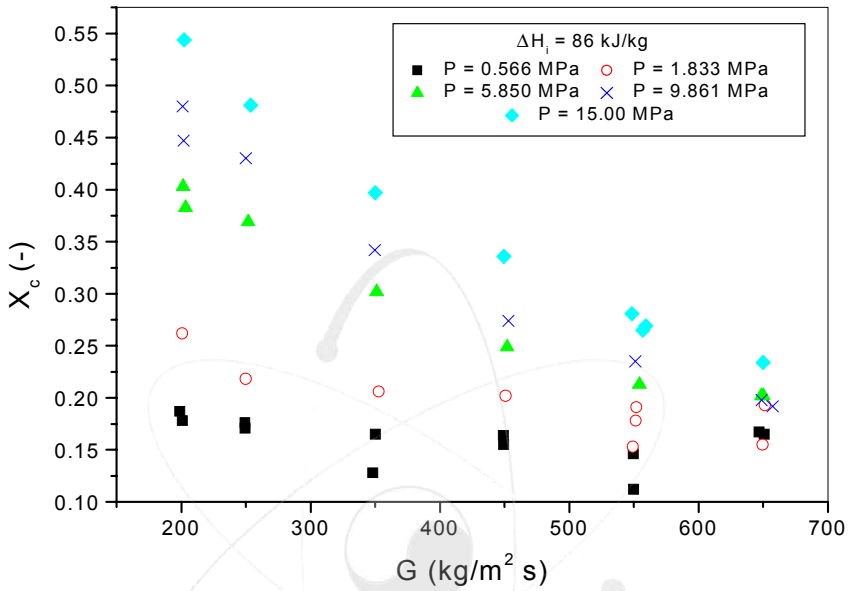

Fig. IV-4. Effect of mass flux on the critical quality (Δh_i = 86 kJ/kg)

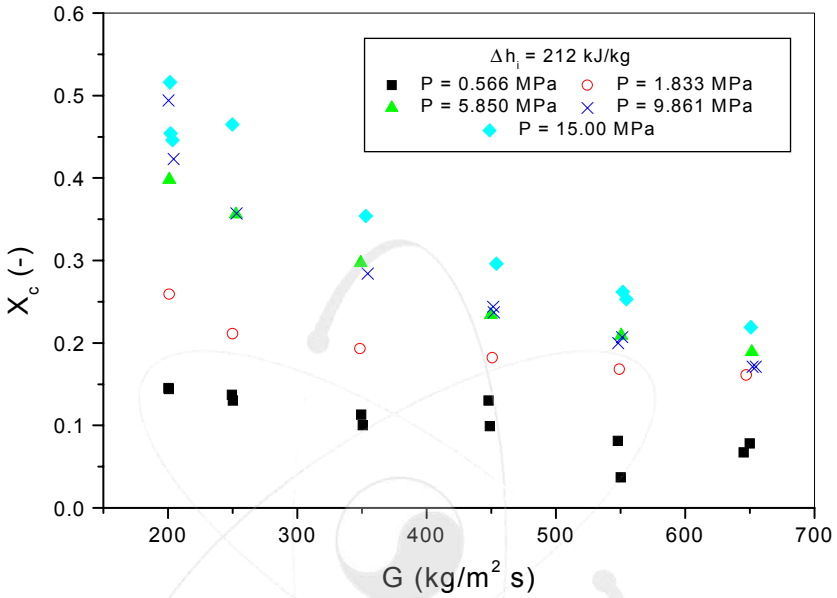

Fig. IV-5. Effect of mass flux on the critical quality (Δh_i = 212 kJ/kg)

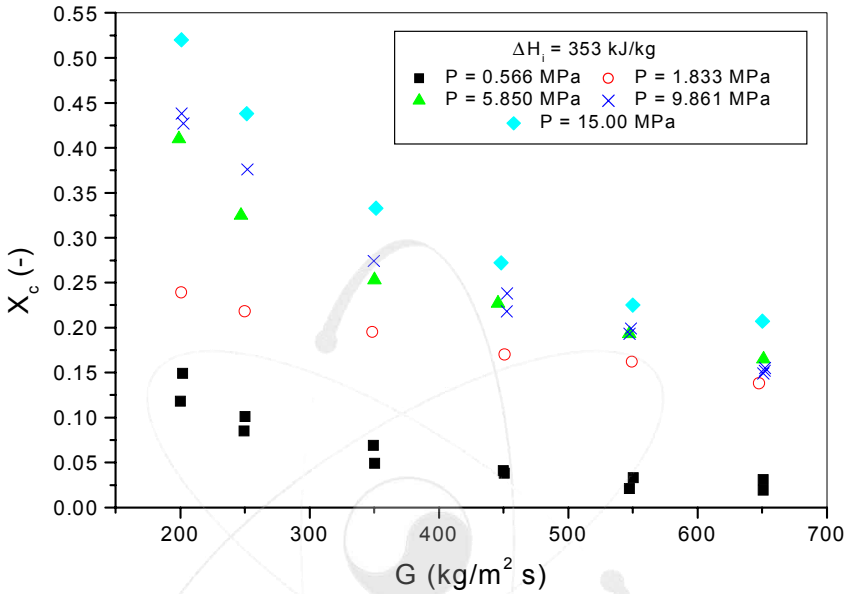

Fig. IV-6. Effect of mass flux on the critical quality (Δh_i = 353 kJ/kg)

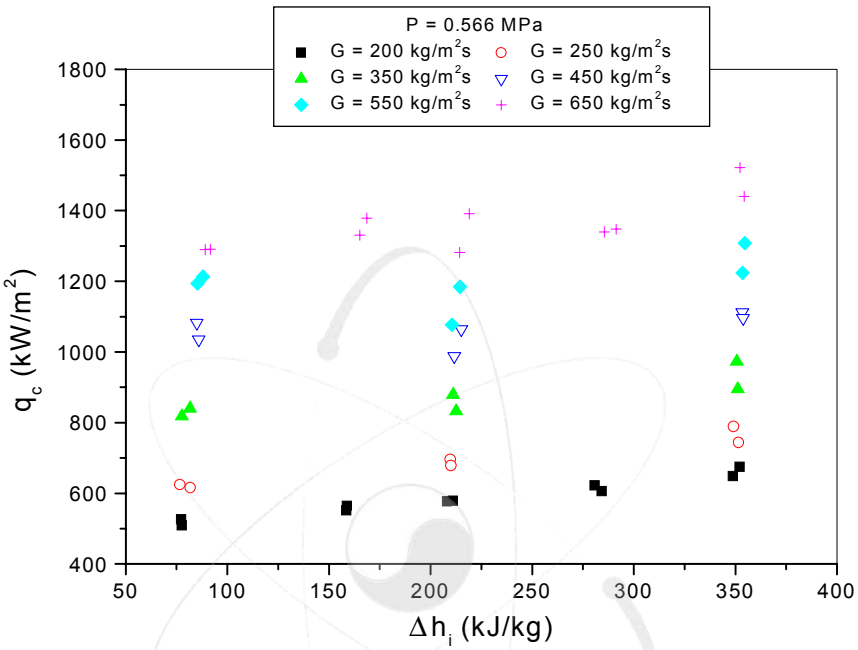

Fig. IV-7. Effect of inlet subcooling on CHF (0.566 MPa)

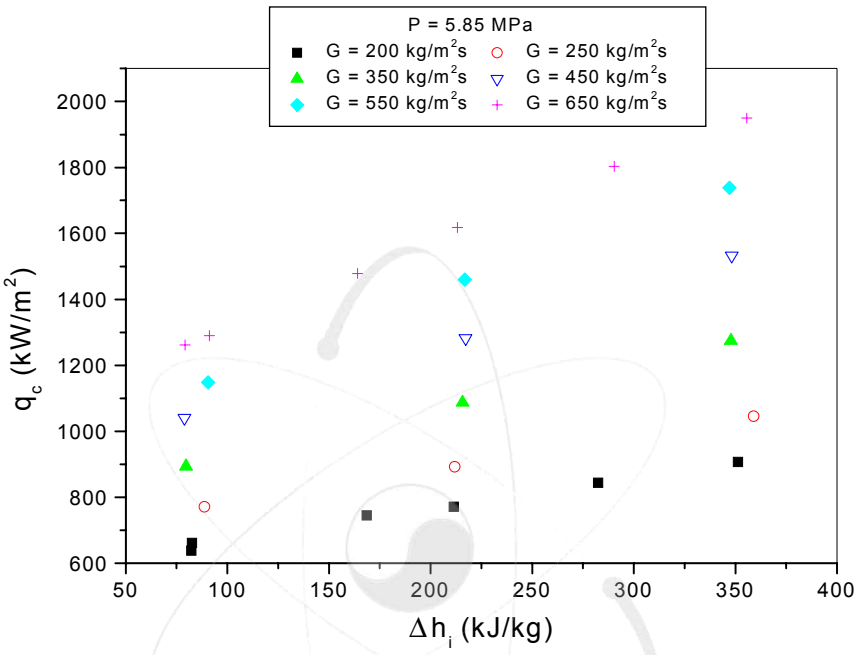

Fig. IV-8. Effect of inlet subcooling on CHF (5.85 MPa)

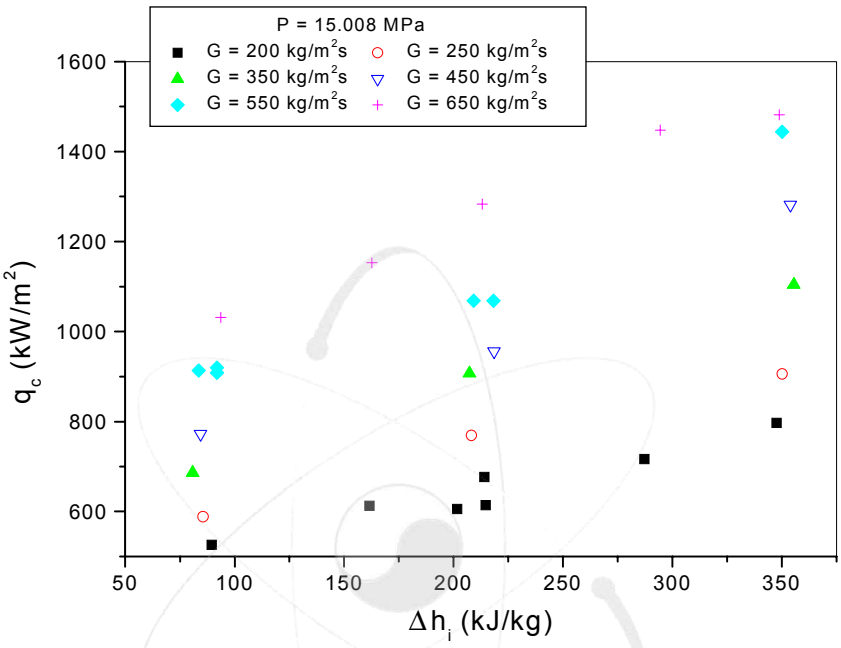

Fig. IV-9. Effect of inlet subcooling on CHF (15.008 MPa)

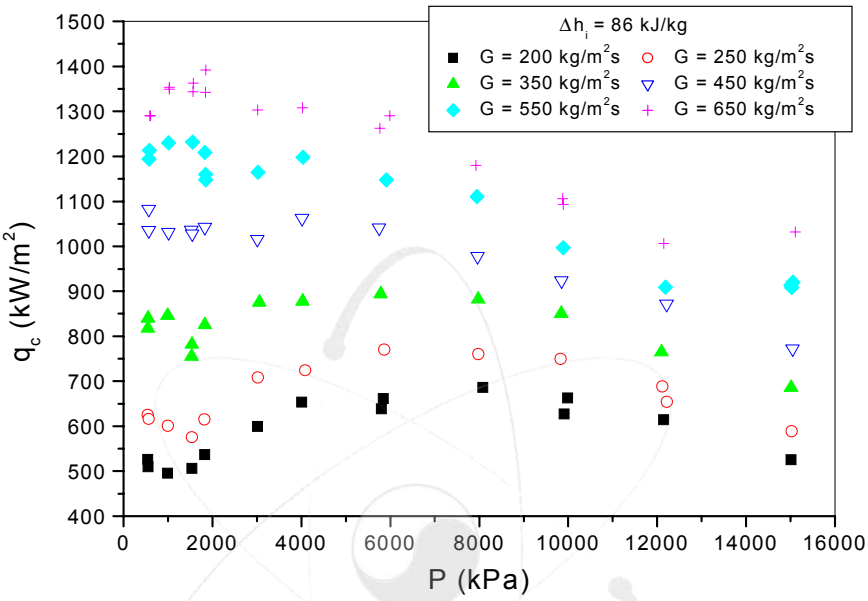

Fig. IV-10. Effect of system pressure on CHF (Δh_i = 86 kJ/kg)

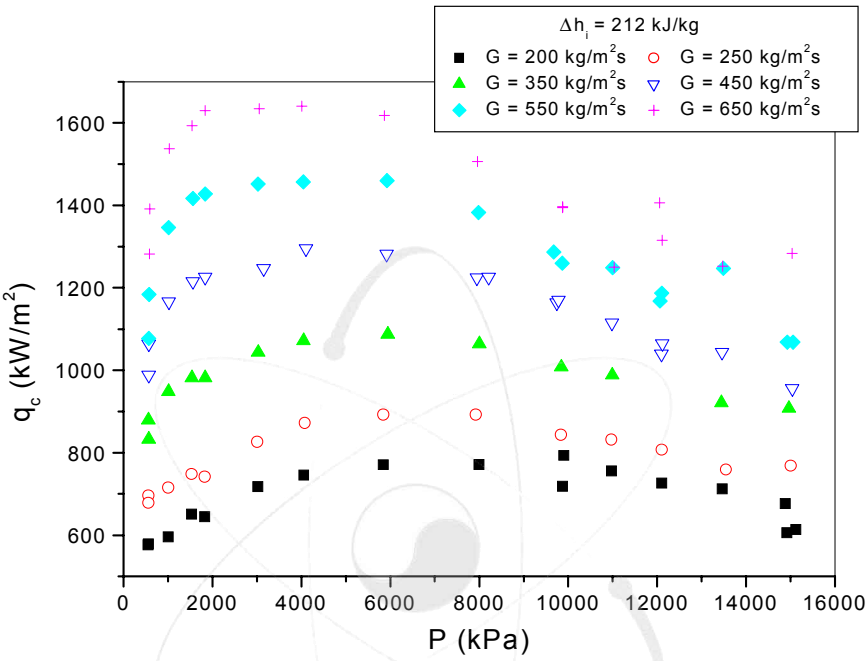

Fig. IV-11. Effect of system pressure on CHF (Δh_i = 212 kJ/kg)

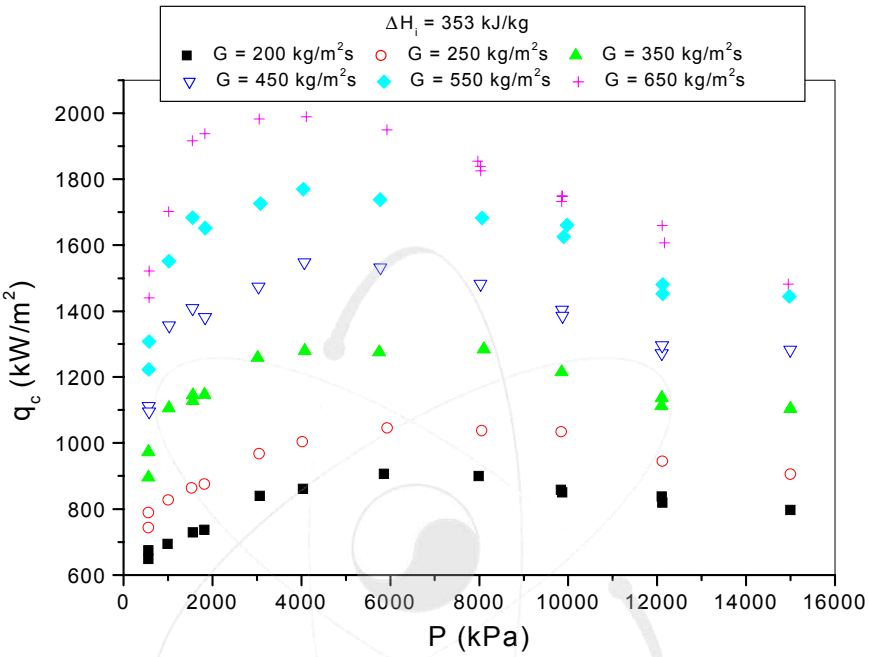

Fig. IV-12. Effect of system pressure on CHF (Δh_i = 353 kJ/kg)

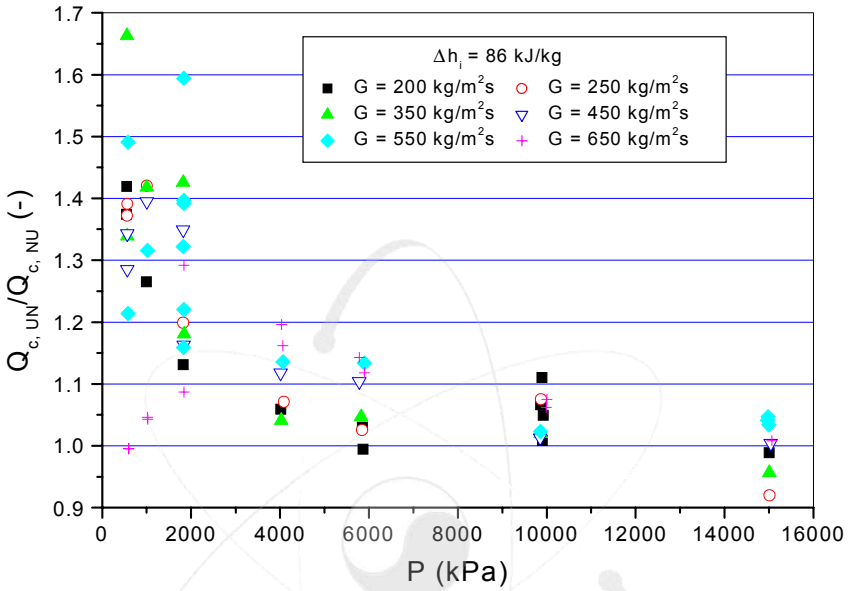

Fig. IV-13. Ratio of critical power vs. pressure (Δh_i = 86 kJ/kg)

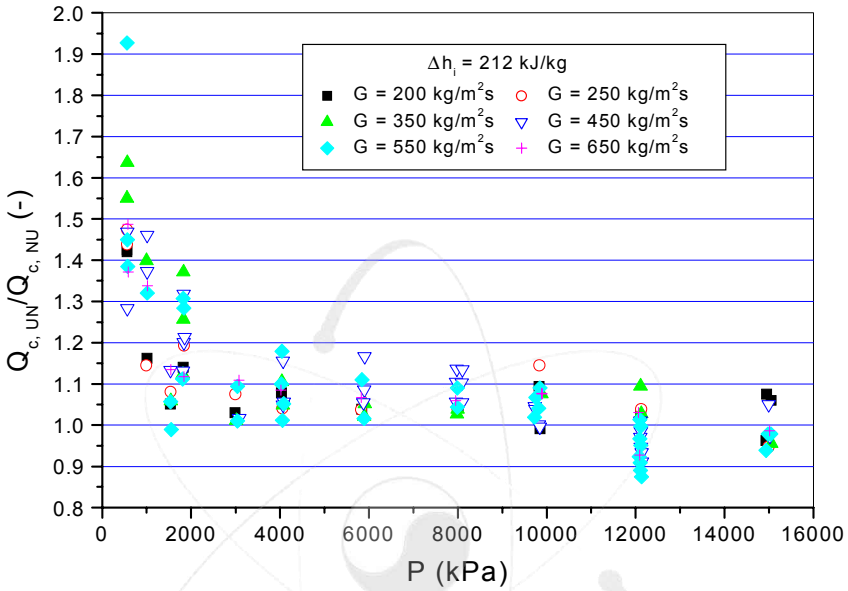

Fig. IV-14. Ratio of critical power vs. pressure (Δh_i = 212 kJ/kg)

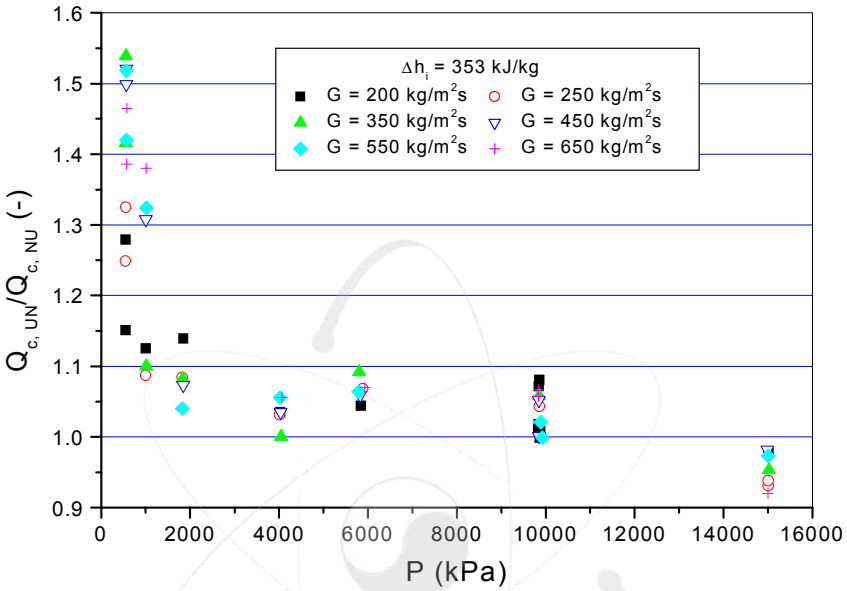

Fig. IV-15. Ratio of critical power vs. pressure (Δh_i = 353 kJ/kg)

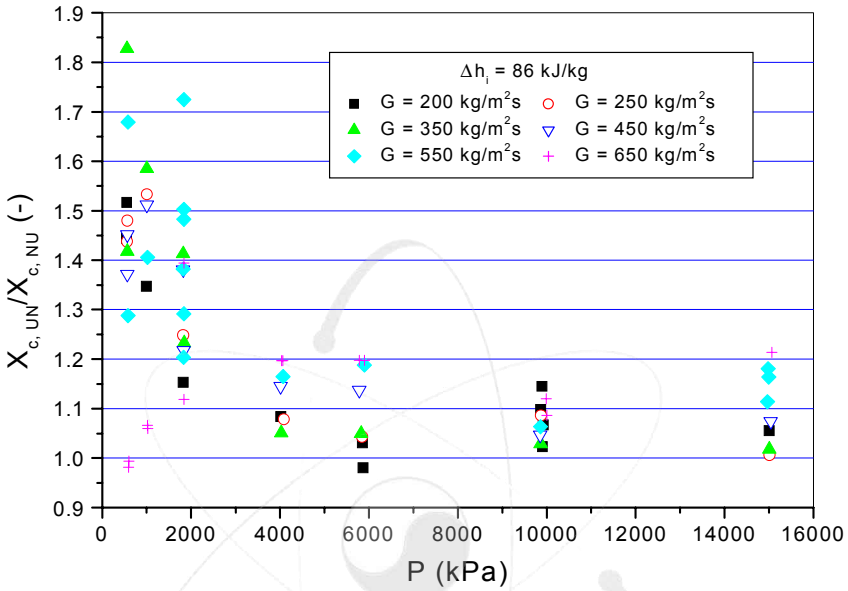

Fig. IV-16. Ratio of critical quality vs. pressure (Δh_i = 86 kJ/kg)

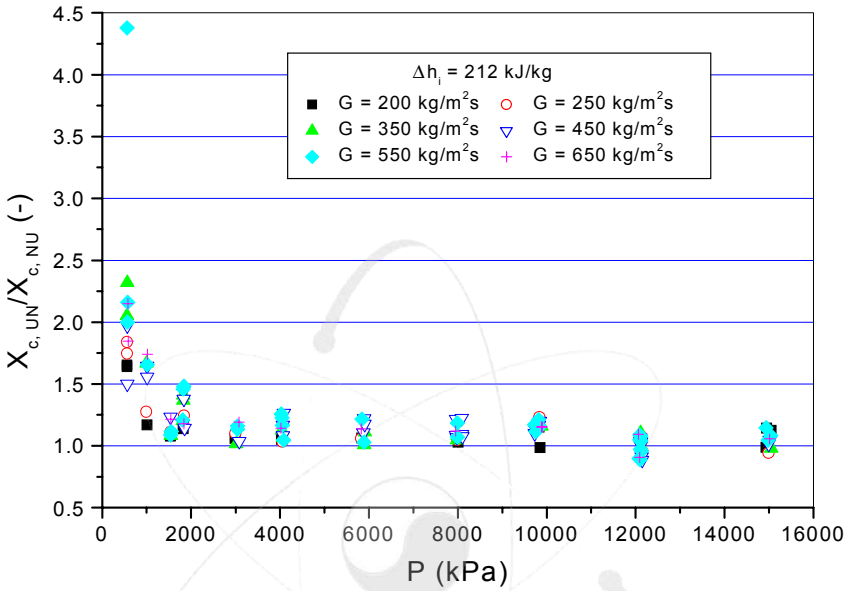

Fig. IV-17. Ratio of critical quality vs. pressure (Δh_i = 212 kJ/kg)

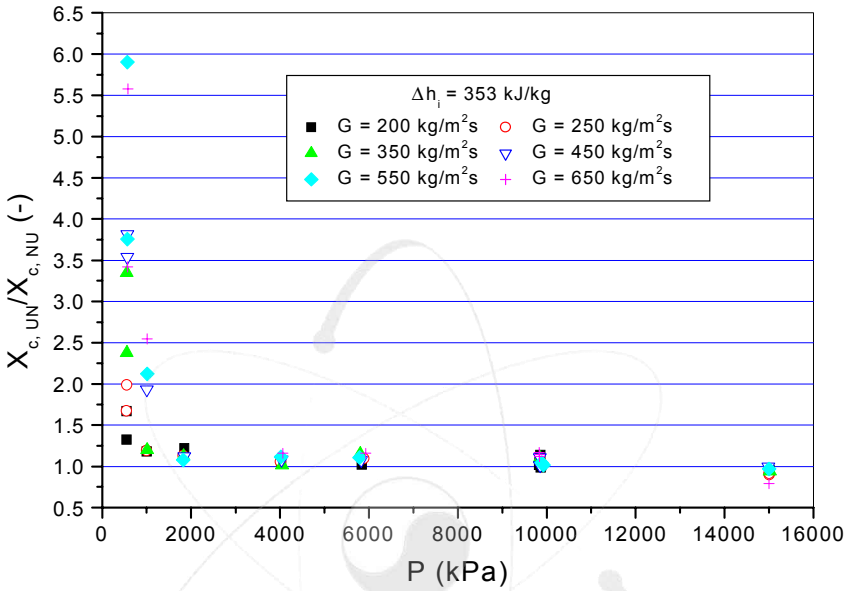

Fig. IV-18. Ratio of critical quality vs. pressure (Δh_i = 353 kJ/kg)

V. Zero-Flow CHF Experiment

V.1 Introduction

Correct characterization of the critical heat flux (CHF) is of particular interest when predicting nuclear reactor core behavior in accident situations, including a flow transient such as reactor circulation pump failure and a loss of coolant accident (LOCA). The core coolant flow is reduced during a large portion of several types of accident scenarios, and the reactor core encounters a stagnant or reverse flow. An understanding of the fundamental nature of the CHF in the vertical flow channel under stagnant or zero flow condition will be important for reactor safety, as is the case with low flow CHF. In the case of a vertical channel with a larger liquid volume or shorter heated section, it may be inferred easily that the CHF mechanism becomes similar to the departure from nucleate boiling (DNB) in pool boiling. The CHF mechanism for a narrow and long vertical channel under a zero flow condition may be different from that of the pool boiling CHF.

Several investigators (Barnard et al., 1974; Mishima and Nishihara, 1987; El-Genk et al., 1988; Chang et al., 1991; Park et al., 1997) have conducted experiments on CHF under very low flow conditions from several hundred kg/m2s to a zero inlet flow with a completely closed bottom end. They have observed that a countercurrent flow is formed in the vertical flow channel at zero and very low flow rates, and subsequently the CHF occurs due to the countercurrent flow limitation (CCFL) or flooding. The CHF in these boiling systems was considerably smaller than that of normal pool boiling (Mishima and Nishihara, 1987; El-Genk et al., 1988). The experiments of El-Genk et al. (1988) indicated that the CHF values with zero flow were about 30 % lower than those with net water upward flow when extrapolated to zero flow. For practical applications in the non-nuclear industry, many studies on the CHF phenomenon of the countercurrent flow of a heated vertical tube closed at the bottom end have been made with respect to the design and performance of closed two-phase thermosyphons (Sakhuja, 1973; Tien and Chung, 1979; Nejat, 1981; Imura et al., 1983; Dobran, 1985; Reed and Tien, 1987; Casarosa and

Dobran, 1988; Katto and Hirao, 1991; Katto and Watanabe, 1992). In these references, flooding in the countercurrent flow was regarded and discussed by many investigators as one of the CHF mechanisms, and empirical flooding equations were employed in the development of the correlations for prediction of the CHF. Hence, the CHF of this sort is called the flooding CHF. The flooding CHF correlations were based on the Wallis empirical equation (Wallis, 1969) obtained from the countercurrent flow in a water and air two-phase system or the Kutateladze criterion for the onset of flooding, with the assumption of mass and energy balance.

The thermal hydraulics system codes most widely used for analyzing accidents in nuclear power plants are RELAP5/MOD3 (RELAP5 code manual, 1995) and TRAC-PF1 (Liles et al., 1984). In these codes, the Biasi correlation (Biasi et al., 1967) and the AECL-UO CHF Look-up table (Groeneveld et al., 1986), which are based on the data base of normal upward flow CHFs in tubes, are employed for the prediction of CHF. To provide the CHF value for the zero flow conditions, the Biasi correlation is evaluated at a mass flux of 200 kg/m2s and the CHF Look-up table uses the Zuber-Griffith pool boiling CHF correlation (Griffith et al., 1977). It is obvious that the codes adopt inappropriate methods to predict the CHF under zero flow conditions. Experimental studies of the CHF in closed two-phase thermosyphons have been made using a uniformly heated vertical tube without a liquid reservoir at the top of the heated section. The conditions of the nuclear reactor may require a vertical test channel with the non-uniformly heated section and the liquid reservoir.

In the above references, the CHF experiments were carried out under near atmospheric pressure conditions. The authors have conducted the CHF experiments for zero inlet flow in a uniformly heated vertical annulus with a liquid reservoir under high pressure conditions (Chun et al., 2000). Until now, CHF experiments in a flow channel with a non-uniformly heated section under high pressure conditions have not been carried out, as far as the authors know. Therefore, this paper presents the results from CHF experiments carried out at zero inlet flow in the annulus flow channel with

uniformly and non-uniformly heated sections and with the water reservoir under extended pressure conditions. Several existing correlations for the countercurrent flooding CHF are compared with the CHF data obtained in the present experiments to examine the applicability of the correlations.

V.2 Experiment Descriptions

The KAERI RCS loop that was described in detail in section II was used to perform the zero-flow CHF experiment. Two kinds of test sections, that is, with uniform heat flux or non-uniform heat flux profiles are used to investigate the axial heat flux profile on the zero-flow CHF. Also, these test sections are described in section II.

The CHF experiments have been performed by the following procedure. First, the circulation pump, preheater and pressurizer are operated for raising the temperature of the loop and establishing inlet subcooling and pressure of the test section at the desired levels, and the isolation valve located at the upper stream of test section is fully closed. Power is applied to the heater rod of the test section and increased gradually in small steps. The period between the power steps is chosen to be sufficiently long (about twenty minuets) so that the loop can stabilize at the steady-state conditions. The water temperatures (T/C 4 and 5, see Fig. V-1) in the upper plenum of the test section and the connecting pipe between the upper plenum and the steam/water separator reach the saturated temperature as the power to the heater rod increases. A countercurrent flow is then formed in the heated section. Namely, a balance of the steam generation in the heated section and the falling saturated water into the heated section from the upper plenum due to gravity is kept. As the loop approaches a CHF condition, the temperature fluctuation of the heater rod surface is detected. The CHF condition in the present experiments is determined when the surface temperature of the heater rod continuously rises and then becomes 100 K higher than the saturation temperature. Whenever the CHF was detected, the heater power was automatically reduced or tripped to prevent any damage to the heater rod.

In the present experimental conditions, the water temperature (T/C 2) at the bottom end of the heated section remained in a subcooled condition, even after power was applied to the heater rod. This is due to some heat loss and convective heat transfer toward the lower plenum. A pressure rise at the upper plenum was not observed during a run of the experiment, since the amount of steam generated in the heated section is considerably smaller, compared to the volume of the steam/water separator. A total of 135 CHF data were obtained in the ranges of the water subcooling enthalpies from 85 to 413 kJ/kg at the bottom end of the heated section and system pressures from 0.52 to 14.96 MPa. The pressure at the top end of the heated section is specified as the system pressure and is used for the analysis of the experimental data.

V.3 Results and Discussion

V.3.1 Data reduction

In the flooding phenomenon for countercurrent flow, the vapor flow rate is the most important parameter. As mentioned above, the water at the bottom part of the heated section is under a subcooled condition at the occurrence of a CHF. In this situation, the amount of steam generated in the heated section cannot be evaluated directly from the mass and energy balances. Information for the locations of the onset of saturated boiling is required to evaluate the vapor flow rate at the top end of the heated section.

We can consider a countercurrent annular flow as illustrated in Fig. V-2. In order to search for the locations of the onset of saturated boiling in the present boiling system, it is assumed that the pressure losses due to friction and acceleration can be neglected for the pressure difference ΔP between the bottom end of the heated section (Z=0) and location Z, and that the void fraction in the subcooled boiling region is negligibly small. The pressure difference ΔP is equal to the static head from the bottom end of the heated section to location Z. Consequently, the average void fraction α from the bottom end (Z=0) to location Z is given as

$$\alpha = \frac{\rho_{l,sat} g Z + (\rho_{l,sub} - \rho_{l,sat}) g Z_{sat} - \Delta P}{(\rho_g - \rho_{l,sat}) g (Z - Z_{sat})}, \quad (1)$$

where ρ_l and ρ_g are the liquid and vapor densities, and g is the gravitational acceleration. The subscripts *sub* and *sat* denote the subcooling and saturation conditions, respectively.

For the present test section, the pressure difference $\Delta P_{m\text{-}2}$ measured by the differential pressure transmitter DP-2 (see Fig. V-1) are plotted as a function of subcooling temperature ΔT_{sub} at the bottom end of the heated section for a given system pressure in Fig. V-3. In the present conditions, it was observed that the relationship between $\Delta P_{m\text{-}2}$ and ΔT_{sub} is linear for a fixed system pressure. The pressure difference $\Delta P_{m\text{-}2,sat}$ for ΔT_{sub} = 0 (i.e., Z_{sat} = 0) at the bottom end of the heated section can be given from the extrapolation of the linear relationship between $\Delta P_{m\text{-}2}$ and ΔT_{sub}. Substituting the value of $\Delta P_{m\text{-}2,sat}$, Z (in the present case, Z = 1.042 m) and Z_{sat}= 0 into Eq. (1), the average void fraction α_0 for the saturated condition at the bottom end of the heated section is calculated for each system pressure. When it is assumed that α decreases linearly in proportion to the increase of distance Z_{sat} from the bottom end of the heated section to the saturation point, the void fraction α is expressed as follows:

$$\alpha = \alpha_0 \left(1 - \frac{Z_{sat}}{Z}\right). \quad (2)$$

Location Z_{sat} of the onset of saturated boiling is given from Eqs. (1), (2) and the measured pressure difference $\Delta P_{m\text{-}2}$. For calculating Eq. (1), the subcooled liquid density $\rho_{l,sub}$ in the bottom region of the heated section uses that for an average of the temperature at the bottom end of the heated section and the saturated temperature.

Subsequently, the boiling length L_B at CHF conditions is defined using the heated length L_h as follows:

$$L_B = L_h - Z_{sat}. \quad (3)$$

The average CHF $q_{C,B}$ over the boiling length is expressed by

$$q_{C,B} = \frac{1}{L_B}\int_{Z_{sat}}^{L_h} q(z)dz, \quad (4)$$

where $q(z)$ is the axial heat flux profile of the heater rod. In the present work, the experimental data are discussed and analyzed with the boiling length L_B and the average CHF $q_{C,B}$.

V.3.2. Observation of CHF behaviors

In the present experiments, the power input to the heater rod was carefully increased. If the power was rapidly increased and the periods between the power steps were short before the water temperature in the upper plenum reached the saturation temperature, rapid temperature rises (i. e. dryout) throughout the surface of the heater rod at the same time were frequently observed in low heat flux conditions (about one half of $q_{C,B}$). This phenomenon is due to the sudden evaporation of water in all regions of the heated surface area under unstable conditions, while the stable countercurrent flow does not form yet. This situation is not desired in the present work, because it is an irregular event relating to an unbalance between the fall of condensed water from the upper plenum and rising vapor in the heated section.

Figure V-4(a) shows the typical surface temperature variation of the heater rod at CHF conditions. As the power level approaches the CHF, the fluctuations of the surface temperature start in the upper region of the heated section (i. e. T/C 1, 2 or 3). When the power level reaches the CHF condition, the magnitude of the temperature fluctuations becomes large and after a while, CHF occurs in the upper region of the heated section. The surface temperature variation shown in Fig. V-4(b) is different from that in Fig. V-4(a). The surface temperatures rise monotonously without the fluctuations after a small temperature fluctuation starts. This type of temperature behavior was observed only at high pressures of 12.08 and 14.96 MPa. In the present experiments, the CHF always occurred at the locations of 10 and 30 mm (T/C 1 and 2) from the top end of the heated section for the uniform heat flux. For the non-uniform heat flux, the CHF occurred mainly at

the locations of 200 mm, and sometimes 10 or 301 mm (T/C 2 and sometimes T/C 1, 3) for the non-uniform heat flux. In the middle positions (T/C 5 and 6), the surface temperatures of the heater rod maintained a constant superheat and temperature fluctuation was not observed during a run of the experiment.

The surface temperature behavior illustrated in Fig. V-4 is closely similar to that observed in Katto and Hiraos experiment (1991), which was conducted in uniformly heated tubes with a liquid reservoir at the top of the heated section. The boiling length varies with the water subcooling condition at the bottom end of the heated section. In Fig. V-5, the CHF values $q_{C,B}$ are given as a function of boiling length to hydraulic equivalent diameter ratio L_B/D_{hy}. The CHF values monotonously decrease with L_B/D_{hy}, although the values for the non-uniform heat flux scatter due to the effect of pressure. This trend is consistent with the analytical and experimental study of Katto and Watanabe (1992), which indicated that the magnitude of the CHF is approximately inversely proportional to the heated length of the tube under a fixed condition of the tube diameter.

However, several experimental studies (Barnard et al., 1974; El-Genk et al., 1988; Imura et al., 1983; Katto and Hirao, 1991) indicated that the CHF in a heated vertical channel with a closed bottom occurs at the middle or lower position of the heated section, in contrast to the results from the observations of the present experiments. For example, Katto and Hirao (1991) reported that the location of the onset of CHF lies between the middle and the bottom end of the heated tubes over a range of L_B/D_{hy} =30 - 112.5. Hwang and Chang (1994) considered a physical model similar to Fig. V-2 for a boiling tube with a closed bottom. They then predicted the CHF locations on the basis of the assumption that dryout occurs at the boundary between the two-phase mixture and the countercurrent annular flow regions, i. e., the location of the minimum liquid film thickness, owing to the evaporation of the falling film. In annulus, if the falling liquid film is formed on both the heated and unheated surface almost uniformly such as that pointed out by Mishima and Nishihara (1987), the amount of downward flow on the unheated surface is

two times as large as that on the heated surface at the top end of the heated section. In the present boiling system, the reason that the CHF occurs at the upper portion of the heated section is presumed as follows. The liquid film is formed at the part above the heated section, and the liquid film flow on the unheated surface reaches a mixture level without evaporation. Even if the flooding begins at the part above the heated section and the falling film flow rate decreases, the mixture level does not go down much because enough water is continuously supplied by the liquid film flow on the unheated surface. The two-phase mixture level exists in a higher position above a location of 510 mm (T/C 5) from the top end of the heated section. As a result, the CHF occurs in the upper region of the heated section.

In order to illustrate the effect of pressure on the CHF in the present boiling system, the measured CHF are plotted as a function of pressure in Fig. V-6. The scattering of the CHF values for a fixed pressure is due to the effect of the boiling length (i. e., the variation of the subcooling at the bottom end of the heated section). The CHFs for the non-uniform heat flux show, over a pressure range of 0.52 to 9.82 MPa, values about 30 % larger than those for the uniform heat flux. For the high pressure region of 12.08 to 14.96 MPa, the trend on the difference of the CHF values between the uniform and non-uniform heat fluxes cannot be recognized due to the insufficiency of the experimental data. In the case of pool boiling, it is known that CHF reaches a maximum at one third of the critical pressure (about 8 MPa) (Morozov, 1962). As can be seen in Fig. V-6, the general trend of the CHF with pressure is that the CHF increases up to a medium pressure of about 6 to 8 MPa with increasing pressure and decreases as the pressure is further increased. This indicates that the CHF behavior with pressure in the present boiling system is closely similar to that of pool boiling, although the magnitude of the CHF variation with pressure is smaller, compared to the case of pool boiling.

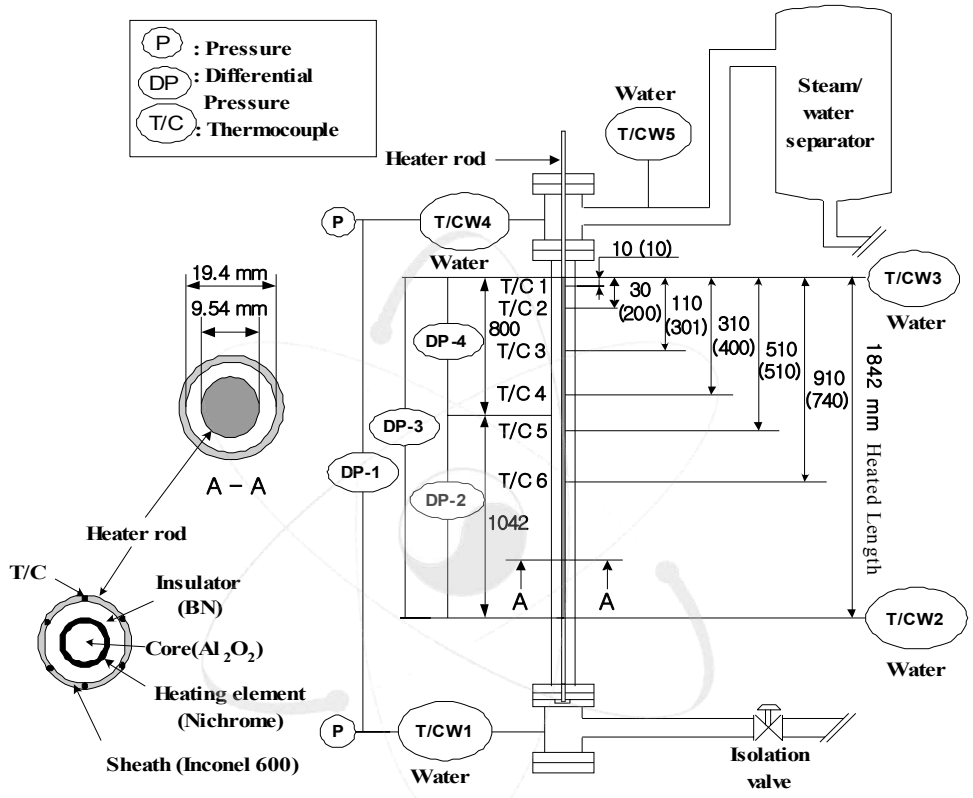

Fig. V-1. Test section geometry and the locations of measuring sensors ( ) denote the thermocouple locations of the heater rod with non-uniform heat flux distribution

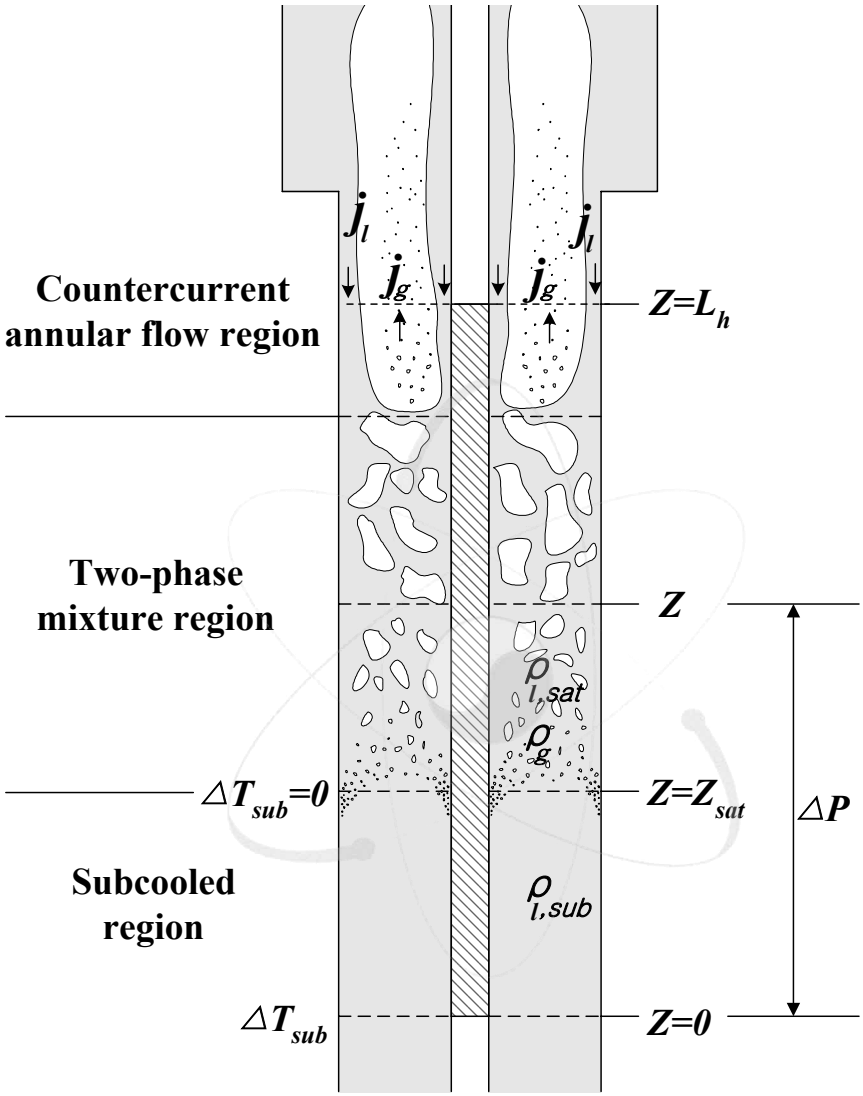

Fig. V-2. Physical model of the present boiling system

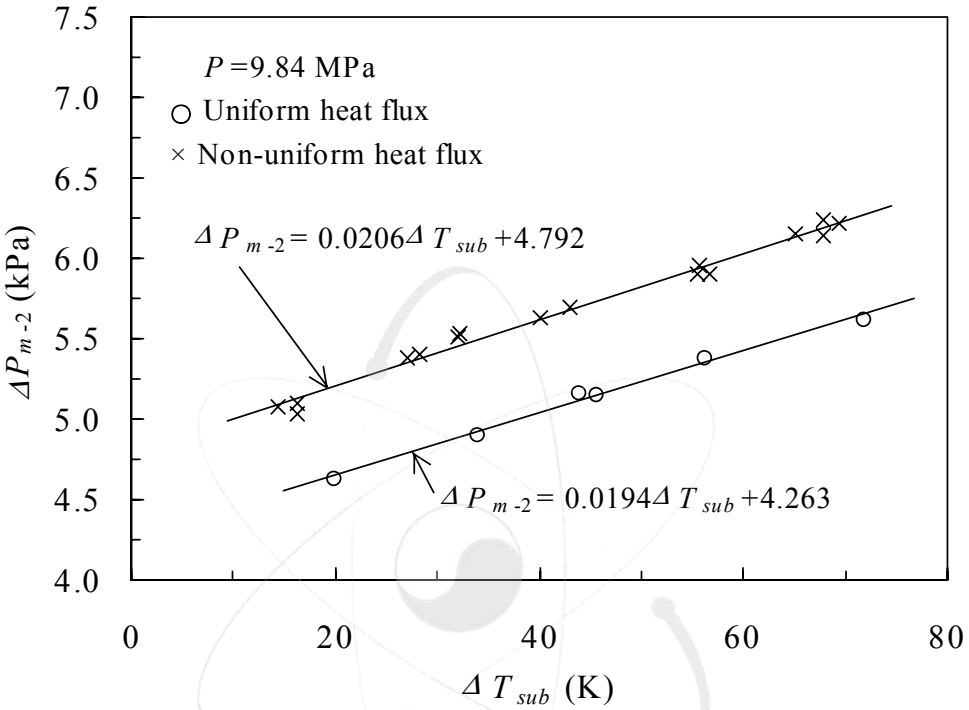

Fig. V-3. Relationship of the pressure drop ($\Delta P_{m\text{-}2}$) and the subcooling temperature at the bottom end of the heated section

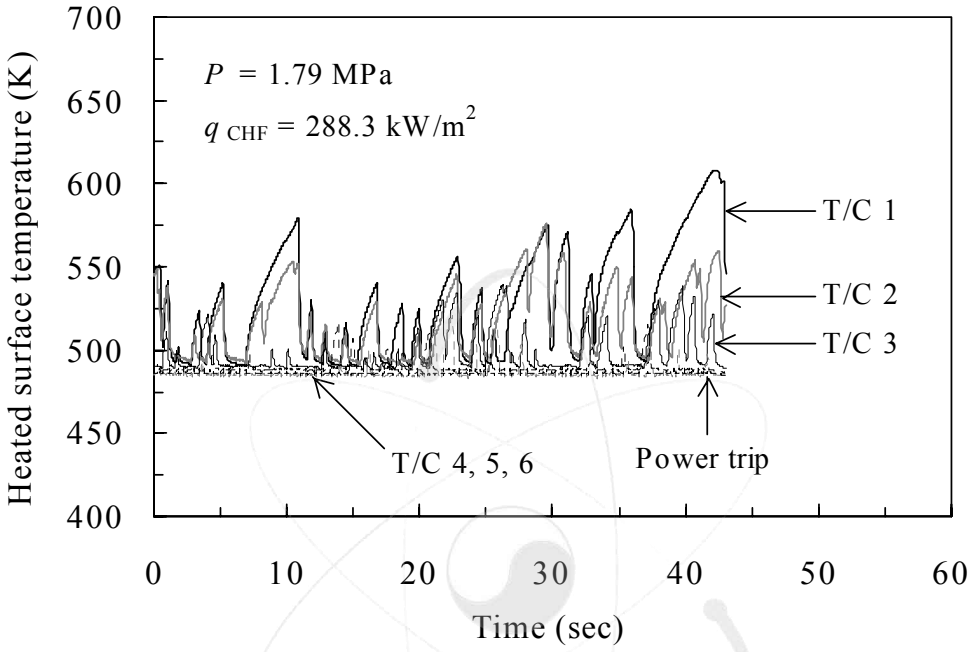

Fig. V-4(a). Typical behavior of the heated surface temperature with time

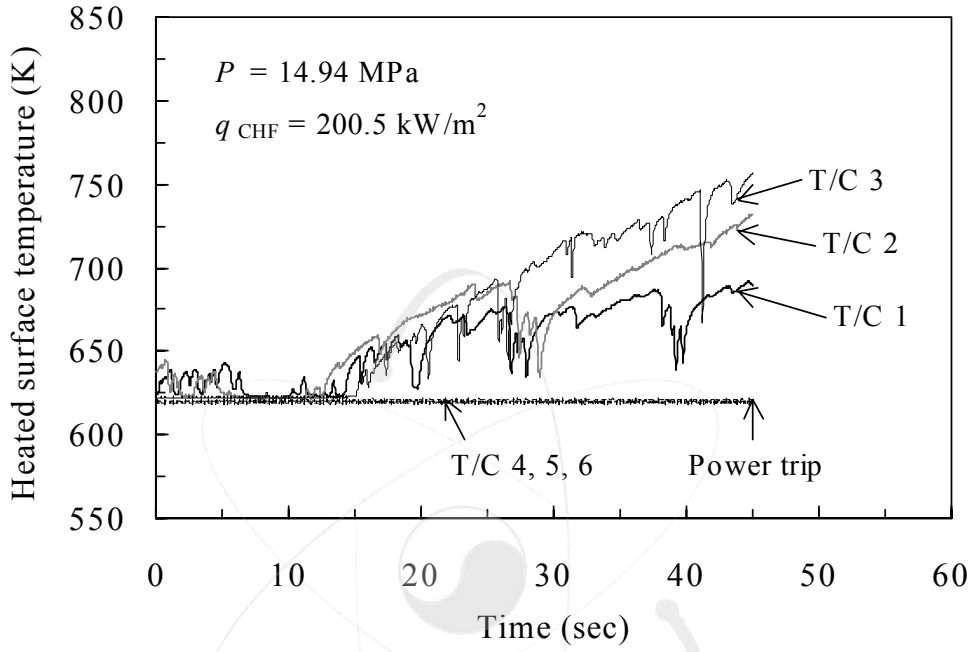

Fig. V-4(b). Temperature behavior of the heated surface at high pressure conditions

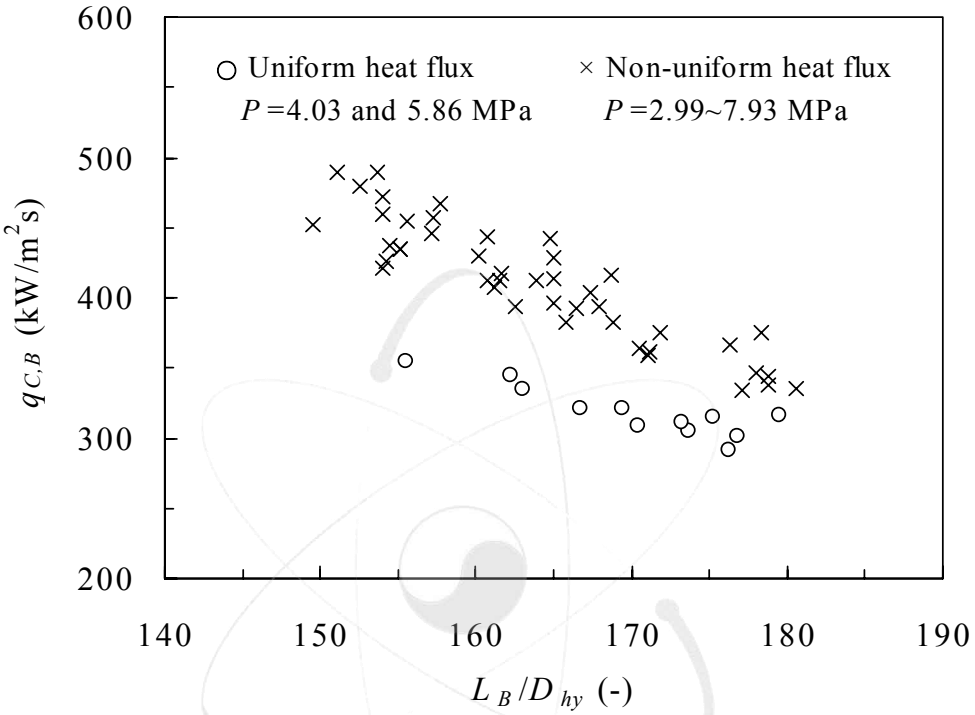

Fig. V-5. Flooding CHF as a function of boiling length to hydraulic equivalent diameter ratio

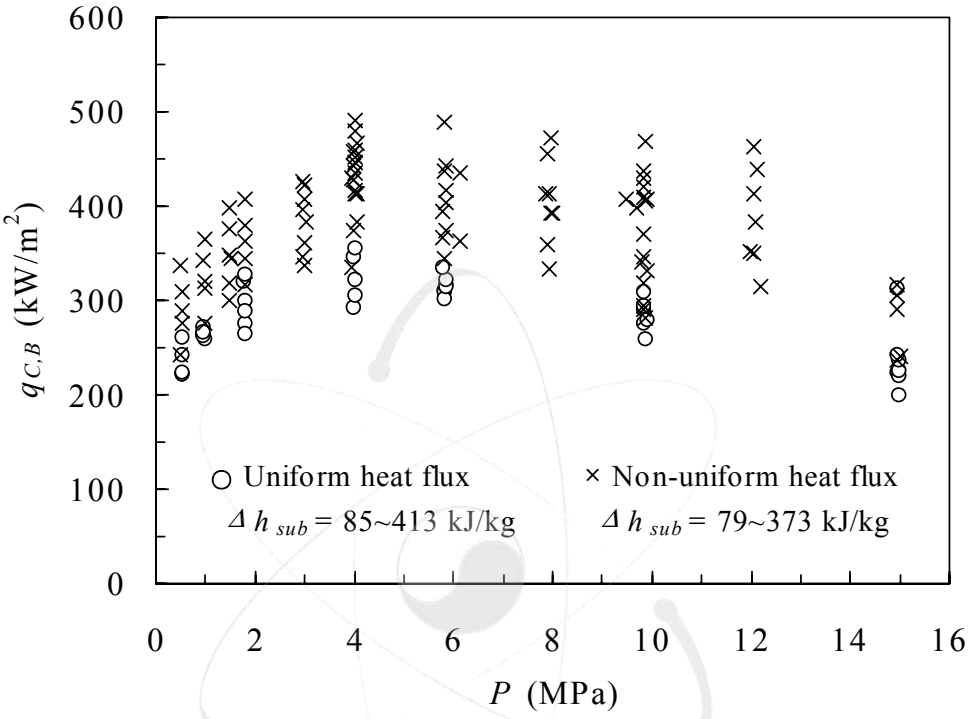

Fig. V-6. Effect of pressure on flooding CHF

VI. Conclusion

A critical heat flux experiment was carried out in water under zero-flow and low-flow conditions using the KAERI RCS CHF loop facility with uniformly and non-uniformly heated vertical annuli. These data provide a valuable base for comparisons of theoretical predictions and correlations, and developments of a new correlation or theoretical models, especially in low-flow conditions. The total number of data generated up to now are as follows:

- low-flow data with uniformly heated vertical annulus : 242
- low-flow data non-uniformly heated vertical annulus : 290
- zero-flow data with uniformly heated vertical annulus : 41
- zero-flow data with non-uniformly heated vertical annulus : 94.

The parametric trends of the CHF are consistent with previous understanding. However, the pressure effect on the CHF shows a complex trend under low-pressure conditions. Also, the effect of the axial heat flux on the CHF is dominant at low-pressure conditions. Other analysis results and comparison with existing correlations can be found in references written by the present authors.

References

ANSI/ASME PTC 19.1, (1985), ASME performance test codes, supplement on instruments and apparatus, part 1, measurement uncertainty.

Barnard, D. A., Dell, F. R. and Stinchcombe, R. A., (1974), Dryout at low mass velocities for an upward boiling flow of refrigerant-113 in a vertical tube, UKEA, AERE-R 7726.

Barnett, P. G., (1966), A correlation of burnout data for uniformly heated annuli and its use for predicting burnout in uniformly heated rod bundles, AEEW-R463.

Becker, K. M., Hernborg, G., Bode, M. and Eriksson, O., (1965), Burnout data for flow of boiling water in vertical round ducts, annuli and rod clusters, Aktiebolaget Atomenergi, Stockholm, Sweden, AE-177.

Biasi, L., Clerici, G. C., Garibba, S., Sala, R. and Tozzi, A., (1967), Studies on burnout. Part 3 - a new correlation for round ducts and uniform heating and its comparison with world data, *Energia Nucleare*, 14, 530-537.

Bowring, R. W., (1977), A new mixed flow cluster dryout correlation for pressures in the range 0.6-15.5 MN/m2 (90-2500 psia) for use in a transient blowdown core, Paper C217/77, *Presented at Conf. On Heat and Fluid Flow in Water Reactor Safety*, IMechE, Manchester, Sep. 13-15.

Casarosa, C. and Dobran, F., (1988), Experimental investigation and analytical modeling of a closed two-phase thermosyphon with imposed convection boundary conditions, *Int. J. Heat Mass transfer*, **31**, 1815-1833.

Chang, S. H., Baek, W. P. and Bae, T. M., (1991), A study of critical heat flux for low flow of water in vertical round tube under low pressure, *Nucl. Eng. Des*. **132**, 225-237.

Chun, S. Y., Cha, J. H. et al., (1997), Critical heat flux for vertical annulus flow channel under low flow and high pressure conditions, *Proc. of 8th Int. Topical Meeting on Nuclear Thermal-Hydraulics*, Vol.2, pp.691-698, Kyoto.

Chun, S. Y., Chung, H. J., Hong, S. D., Yang, S. K. and Chung, M. K., (1998), Effect of pressure on critical heat flux in vertical annulus flow channel under low flow conditions, *Proc. of first Korea-Japan Symposium on Nuclear Thermal Hydraulics and Safety* (NTHAS98), pp. 342-347, Pusan, Korea, October.

Chun, S. Y., Chung, H. J., Hong, S. D., Yang, S. K. and Chung, M. K., (2000a), Critical heat flux in uniformly heated vertical annulus under a wide range of pressure 0.57 to 15.0 MPa, *Journal of the Korean Nuclear Society*, **32**, 128-141.

Chun, S. Y., Moon, S. K., Chung, H. J., Yang, S. K., Chung, M. K., (2000b), Critical heat flux under zero flow conditions in vertical annulus with uniformly and non-uniformly heated sections, *Paper submitted for Publication in Nucl. Eng. & Design*.

Dobran, F., (1985), Steady-state characteristics and stability thresholds of a closed two-phase thermosyphon, *Int. J. Heat Mass Transfer*, **28**, 949-957.

Doerffer, S., Groeneveld, D. C., Cheng, S. C., Rudzinski, K. F., (1994), A comparison of critical heat flux in tubes and annuli, *Nucl. Eng. Design*, **149**, 167-175.

El-Genk, M. S., Haynes, S. J. and Kim, S. H., (1988), Experimental studies of critical heat flux for low flow of water in vertical annuli at near atmospheric pressure, *Int. J. Heat Mass Transfer*, **31**, 2291-2304.

Griffith, P., Pearson, J. F. and Lepowski, R. J., (1977), Critical heat flux during a loss-of-coolant accident, *Nuclear Safety*, **18**, 298-305.

Groeneveld, D. C., Cheng, S. C. and Doan, T., (1986), 1986 AECL-UO CHF look-up table, *Heat Transfer Eng.*, **7**, 46-62.

Groeneveld, D. C., Leung, L. K. H., Kirillow, P. L. et al., (1996), The 1995 look-up table for critical heat flux in tubes, *Nucl. Eng. Design*, **163**, 1-23.

Hwang, D. H. and Chang, S. H., (1994), Development of a phenomenological model for the prediction of dryout locations under flooding-limited critical heat flux conditions, *Nucl. Eng. Design*, **148**, 475-486.

Imura, H., Sasaguchi, K., Kozai, H. and Numata, S., (1983), Critical heat flux in closed two-phase thermosyphon, *Int. J. Heat Mass Transfer*, **26**, 1181-1188.

Janssen, E. and Kervinen, J. A., (1963), Burnout conditions for single rod in annular geometry, water at 600 to 1400 psia, General Electric Company, Atomic Energy Commission, USA, GEAP-3899.

Katto, Y. and Hirao, T., (1991), Critical heat flux of counter-flow boiling in a uniformly heated vertical tube with a closed bottom, *Int. J. Heat Mass Transfer*, **34**, 993-1001.

Katto, Y. and Watanabe, K., (1992), An analytical study on the critical heat flux of countercurrent boiling in a vertical tube with a closed bottom, *Int. J. Heat Mass Transfer*, **35**, 3021-3028.

Kumamaru, K., Koizumi, Y. and Tasaka, K., (1990), Critical heat flux for annulus under high-pressure, low-flow and mixed inlet conditions, *J. Nucl. Sci. Tech.*, **27**[1], 68-80.

Liles, D. R. et al., (1984), TRAC-PF1, An advanced best-estimate computer program for pressurized water reactor analysis, Draft, Los Alamos National Laboratory.

Mishima, K. and Ishii, M., (1982), Experimental study on natural convection boiling burnout in annulus, *Proc. of the 7th International Heat Transfer Conf.*, Munchen, Vol.4, pp.309-314.

Mishima, K. and Ishii, M., (1984), Flow regime transition criteria for upward two-phase flow in vertical tubes, *Int. J. Heat Mass Transfer*, **27**[5], 723-737.

Mishima, K. and Nishihara, H., (1987), Effect of channel geometry on critical heat flux for low pressure water, *Int. J. Heat Mass Transfer*, **30**, 1169-1182.

Moon, S. K., Chun, S. Y., Chung, H. J., Yang, S. K., and Chung, M. K., (2000), Effect of axial heat flux distributions on critical heat flux under low flow and a wide range of system pressures with vertical annulus, *Proc. of 8th Int. Conf. on Nuclear Eng. (ICONE 8)*, April 8-12, Baltimore, MD USA.

Morozov, V. G., (1962), New experimental data on critical heat loads at boiling of liquids on a submerged heating surface, *Int. J. Heat Mass Transfer*, **5**, 661-666.

Nejat, Z., (1981), Effect of density ratio on critical heat flux in closed end vertical tubes, *Int. J. Multiphase Flow*, **7**, 321-327.

Park, J. W., Baek, W. P. and Chang, S. H., (1997), Critical heat flux and flow pattern for water flow in annular geometry, *Nucl. Eng. Design*, **172**, 137-155.

Reed, J. G. and Tien, C. L., (1987), Modeling of the two-phase closed thermosyphon, *Transaction of the ASME, J. Heat Transfer*, **109**, 722-730.

RELAP5 code manual, NUREG/CR-5535, (1995), Idaho National Engineering and Environment Laboratory, USNRC.

Rogers, J. T., Salcudean, M. and Tahir, A. E., (1982), Flow boiling critical heat fluxes for water in a vertical annulus at low pressure and velocities, *Proc. of the 7th International Heat Transfer Conf.*, Munchen, Vol.4, pp.339-344.

Sakhuja, R. K., (1973), Flooding constraint in wickless heat pipes, ASME Paper 73-WA/HT-7.

Schoesse, T., Aritomi, M., Kataoka, Y., Lee, S. R., Yoshioka, Y. and Chung, M. K. (1997), Critical heat flux in a vertical annulus under low upward flow and near atmospheric pressure, *J. Nucl. Sci. Tech.*, 34[5], 559-570.

Tien, C. L. and Chung, K. S., (1979), Entrainment limits in heat pipes, AIAA Journal, 17, 643-646.

Wallis, G. B., (1969), One-dimensional two-phase flow, McGraw-Hill, 336-342.

Weaver, W. L. et al., (1991), The RELAP5/MOD3 code for PWR safety analysis, *Proceeding of the 4th International Topical Meeting on Nuclear Reactor Thermalhydraulics*, Karlsruhe, 2, 1221-1226.

Appendix A. CHF Data Base for Uniformly Heated Vertical Annulus

Low-Flow CHF Data with Uniformly Heated Vertical Annulus

1) Geometry

- Annulus inner diameter : 9.54 mm
- Annulus outer diameter : 19.4 mm
- Heated length : 1842 mm
- Axial heat flux profile : uniform

2) Nomenclature

P_{in} : Inlet pressure
P_{out} : Outlet pressure
G : Mass flux
T_{in} : Inlet water temperature
Δh_i : Inlet subcooling
q_c : CHF
X_c : Exit quality

Run No.	P_{in} (MPa)	P_{out} (MPa)	G (kg/m^2s)	T_{in} (oC)	Δh_i (kJ/kg)	q_c (kW/m^2)	X_c (-)
U_A_1_1	1.830	1.803	543.60	158.20	219.90	1533.50	0.248
U_A_1_2	1.833	1.808	476.10	158.10	220.70	1351.30	0.250
U_A_1_3	1.833	1.808	421.30	159.00	216.81	1230.40	0.263
U_A_1_4	1.817	1.797	383.80	158.20	218.30	1125.70	0.263
U_A_1_5	1.815	1.797	345.30	158.70	215.89	1031.90	0.272
U_A_1_6	1.812	1.797	300.60	162.50	199.04	909.30	0.285
U_A_1_7	1.812	1.783	566.30	159.90	210.32	1560.50	0.244
U_A_1_8	1.813	1.757	458.96	159.49	212.16	1159.62	0.214
U_A_1_9	1.859	1.809	252.38	158.44	222.40	739.98	0.261
U_A_1_10	1.814	1.758	207.07	158.40	217.04	654.60	0.293
U_A_1_11	1.836	1.809	649.03	159.19	216.34	1524.13	0.188
U_A_1_12	1.785	1.723	550.79	160.27	205.39	1327.93	0.203
U_A_1_13	1.874	1.827	496.48	159.38	220.19	1243.02	0.208
U_A_1_14	1.842	1.792	403.64	160.30	212.22	1021.66	0.215
U_A_1_15	1.787	1.738	347.72	159.47	209.11	922.37	0.232
U_A_1_16	1.867	1.823	301.03	160.46	214.55	836.46	0.246
U_B_1_1	1.820	1.790	560.90	189.00	83.72	1336.50	0.263
U_B_1_2	1.815	1.799	301.70	190.50	76.43	779.20	0.289
U_B_1_3	1.810	1.792	381.20	189.50	80.27	984.80	0.290
U_B_1_4	1.815	1.790	470.00	188.90	83.55	1176.00	0.278
U_B_1_5	1.828	1.767	649.12	189.80	81.18	1299.94	0.215
U_B_1_6	1.813	1.781	201.95	189.04	82.72	541.13	0.302
U_B_1_7	1.819	1.764	252.28	189.21	82.71	616.32	0.271
U_B_1_8	1.849	1.785	351.26	188.89	87.75	815.97	0.254
U_B_1_9	1.845	1.791	451.23	189.65	83.91	1013.75	0.246
U_B_1_10	1.829	1.798	552.38	189.42	82.93	1171.64	0.230
U_C_1_1	1.813	1.725	651.19	171.25	160.99	1425.50	0.197
U_C_1_2A	1.817	1.773	201.50	171.09	162.17	561.00	0.273
U_D_1_1A	1.843	1.777	647.31	141.81	292.05	1630.51	0.172
U_D_1_2	1.835	1.787	199.25	142.90	286.45	675.68	0.287
U_E_1_1	1.810	1.751	546.35	126.11	355.07	1530.39	0.175
U_E_1_2	1.857	1.803	450.16	126.61	358.60	1320.56	0.191
U_E_1_3	1.828	1.762	351.50	126.66	354.90	1105.13	0.219

Run No.	P_{in} (MPa)	P_{out} (MPa)	G (kg/m^2s)	T_{in} (oC)	Δh_i (kJ/kg)	q_c (kW/m^2)	X_c (–)
U_E_1_4	1.815	1.766	251.09	125.39	358.75	845.94	0.246
U_E_1_5	1.875	1.798	201.72	127.10	358.78	747.91	0.291
U_E_1_6	1.831	–	649.30	126.37	353.09	1775.89	0.165
U_A_2_1	12.087	12.053	303.61	289.80	210.00	841.20	0.393
U_A_2_2	12.119	12.084	352.05	291.00	204.82	904.40	0.358
U_A_2_3	12.117	12.082	422.19	288.80	216.48	1002.90	0.307
U_A_2_4	12.121	12.084	451.99	290.10	209.72	1042.80	0.299
U_A_2_5	12.121	12.082	502.34	288.60	217.71	1122.40	0.277
U_A_2_6	12.123	12.084	546.15	290.00	210.34	1176.70	0.267
U_A_2_7	12.075	12.074	648.88	289.65	210.24	1212.47	0.208
U_A_2_8	12.094	12.033	549.59	290.19	208.14	1073.12	0.227
U_A_2_9	12.152	12.116	502.57	289.99	211.57	1032.85	0.246
U_A_2_10	12.178	12.140	453.55	290.38	210.56	963.98	0.262
U_A_2_11	12.081	12.088	400.69	290.38	206.55	897.02	0.287
U_A_2_12	12.152	12.112	352.04	290.33	209.74	849.63	0.321
U_A_2_13	12.145	12.131	303.62	289.65	213.12	802.30	0.366
U_A_2_14	12.149	12.057	249.71	289.50	214.08	747.00	0.437
U_A_2_15	12.132	12.136	201.54	290.38	208.66	662.03	0.501
U_A_3_1	4.079	4.049	306.40	205.80	213.57	931.80	0.312
U_A_3_2	4.040	3.996	359.11	205.00	214.40	1056.40	0.297
U_A_3_3	4.077	4.044	410.84	206.50	210.27	1143.60	0.277
U_A_3_4	4.041	4.002	470.83	205.00	214.48	1251.80	0.256
U_A_3_5	4.012	3.972	522.74	205.20	211.50	1340.50	0.244
U_A_3_6	4.037	3.997	566.36	204.80	215.09	1436.70	0.238
U_A_3_7	4.033	3.950	647.61	205.48	211.84	1487.90	0.205
U_A_3_8	4.028	4.017	253.61	205.21	212.68	808.77	0.332
U_A_3_9	4.020	3.928	207.93	205.03	212.76	715.84	0.368
U_A_3_10	4.039	3.975	450.24	205.15	213.72	1135.21	0.236
U_A_3_11	4.123	4.086	549.15	203.72	225.95	1281.93	0.204
U_A_3_12	4.095	4.065	353.20	205.75	214.92	1001.45	0.282
U_A_3_13	4.064	4.011	501.10	204.80	217.13	1232.66	0.226
U_A_3_14	4.089	4.015	398.90	204.93	218.23	1070.53	0.258
U_B_3_1	4.042	3.977	655.03	230.76	96.32	1307.77	0.230
U_B_3_1A	4.099	4.007	649.93	233.62	87.03	1270.76	0.230
U_B_3_2	4.034	3.997	199.08	233.70	81.97	616.40	0.396
U_B_3_3A	4.099	4.051	549.93	233.52	87.49	1137.72	0.246
U_B_3_4	4.019	4.006	451.49	233.78	79.98	992.97	0.269
U_B_3_5	4.027	4.022	348.85	233.26	83.53	813.90	0.286
U_B_3_6	4.096	4.057	250.61	233.53	87.20	691.28	0.346
U_E_3_1	4.008	3.971	648.90	175.38	343.61	1756.65	0.187
U_E_3_2	4.026	4.018	201.12	174.73	347.70	794.02	0.363
U_E_3_3	4.000	3.976	548.90	174.13	348.49	1562.80	0.204
U_E_3_4	4.002	3.957	450.55	174.07	348.85	1339.42	0.222
U_E_3_5	4.018	3.964	351.30	174.82	346.77	1139.88	0.263
U_E_3_6	4.011	4.011	251.02	174.39	348.17	922.63	0.323
U_A_4_1	5.918	5.888	310.37	233.00	204.16	951.70	0.348
U_A_4_2	5.884	5.852	347.38	233.10	201.77	1019.40	0.329
U_A_4_3	5.855	5.818	391.52	232.40	203.40	1090.60	0.304
U_A_4_4	5.877	5.843	436.54	232.30	205.12	1163.50	0.285
U_A_4_5	5.886	5.848	482.84	232.80	203.29	1250.90	0.274
U_A_4_6	5.758	5.720	559.89	233.70	191.78	1355.40	0.254

Run No.	P_{in} (MPa)	P_{out} (MPa)	G (kg/m^2s)	T_{in} (oC)	Δh_i (kJ/kg)	q_c (kW/m^2)	X_c (–)
U_A_4_7	5.796	5.765	653.52	231.89	202.50	1443.92	0.213
U_A_4_8	5.838	5.763	450.07	231.25	207.77	1131.07	0.257
U_A_4_9	5.855	5.768	400.10	231.71	206.75	1046.09	0.274
U_A_4_10	5.839	5.786	300.12	231.03	208.99	909.48	0.336
U_A_4_11	5.807	5.819	252.61	231.45	205.21	824.43	0.374
U_A_4_12	5.841	5.776	200.88	232.01	204.53	713.60	0.420
U_A_4_13	5.857	5.806	550.89	230.18	213.92	1293.96	0.228
U_A_4_14	5.851	5.771	353.40	229.58	216.33	989.65	0.296
U_A_4_15	5.889	5.787	500.30	230.47	214.34	1205.72	0.238
U_B_4_1	5.803	5.758	641.77	257.35	80.87	1206.64	0.240
U_B_4_2	5.906	5.805	203.24	257.28	87.10	585.78	0.394
U_B_4_3	5.890	5.828	552.25	257.28	86.23	1088.54	0.252
U_B_4_4	5.818	5.837	450.46	258.11	77.99	960.54	0.281
U_B_4_5	5.870	5.792	351.36	257.28	85.04	834.07	0.315
U_B_4_6	5.973	5.781	251.17	257.98	87.50	719.78	0.393
U_B_4_6A	5.833	5.771	251.40	257.62	81.77	703.83	0.384
U_C_4_1	5.889	5.834	648.94	240.92	165.19	1350.99	0.219
U_C_4_2	5.819	5.807	203.85	241.37	159.07	664.39	0.405
U_D_4_1	5.859	5.862	649.94	215.56	281.31	1595.67	0.203
U_D_4_2	5.898	5.810	203.29	214.97	286.21	762.05	0.401
U_E_4_1	5.922	5.886	652.28	199.79	356.02	1743.95	0.190
U_E_4_2	5.833	5.792	203.92	199.10	354.13	843.22	0.418
U_E_4_3	5.815	5.814	550.22	199.51	351.23	1546.87	0.214
U_E_4_4	5.871	5.804	450.97	199.59	354.11	1357.07	0.243
U_E_4_5	5.856	5.865	350.60	199.11	355.40	1164.26	0.291
U_E_4_6	5.837	5.793	250.01	198.63	356.44	933.21	0.354
U_A_5_1	8.007	7.974	309.33	254.20	211.34	946.50	0.374
U_A_5_2	7.993	7.954	347.93	254.30	210.18	984.90	0.336
U_A_5_3	7.986	7.954	408.26	254.80	207.42	1067.90	0.301
U_A_5_4	7.973	7.947	443.87	254.30	209.22	1130.10	0.288
U_A_5_5	7.998	7.961	494.07	253.90	212.37	1162.70	0.253
U_A_5_6	7.993	7.954	543.64	254.40	209.70	1260.60	0.249
U_A_5_7	7.942	7.894	648.12	254.07	208.86	1334.99	0.204
U_A_5_8	7.972	7.934	401.02	254.92	206.24	1015.15	0.286
U_A_5_9	7.974	7.926	302.23	253.91	211.08	869.07	0.341
U_A_5_10	8.061	7.967	253.01	253.75	216.04	827.39	0.406
U_A_5_11	8.018	8.018	206.97	254.02	212.81	716.63	0.440
U_A_5_12	7.959	7.933	353.97	254.65	206.85	974.30	0.324
U_A_5_13	7.978	7.867	451.19	252.92	216.20	1080.66	0.257
U_A_5_14	7.989	7.940	551.15	253.71	212.87	1206.66	0.225
U_A_6_1	9.827	9.806	558.23	272.70	202.80	1148.53	0.226
U_A_6_2	9.769	9.712	518.24	272.50	201.40	1096.99	0.237
U_A_6_3	9.710	9.685	450.52	272.20	200.23	1016.59	0.263
U_A_6_4	9.908	9.869	413.08	272.45	207.78	974.34	0.279
U_A_6_5	9.926	9.945	351.61	273.52	203.13	907.48	0.324
U_A_6_6	9.998	9.900	309.32	271.05	218.80	871.57	0.357
U_A_6_7	9.904	9.826	653.08	270.95	215.23	1255.92	0.193
U_A_6_8	9.843	9.799	250.95	271.05	212.05	807.37	0.433
U_A_6_9	9.795	9.712	202.91	271.73	206.52	700.65	0.480
U_B_6_1	10.103	10.051	651.97	295.02	97.20	982.40	0.207
U_B_6_2A	9.826	9.814	202.27	295.80	80.55	595.49	0.482

Run No.	P_{in} (MPa)	P_{out} (MPa)	G (kg/m^2s)	T_{in} (oC)	Δh_i (kJ/kg)	q_c (kW/m^2)	X_c (–)
U_B_6_2B	9.873	9.831	201.84	295.36	85.10	619.81	0.503
U_B_6_3	9.839	9.851	549.91	295.41	83.31	909.05	0.242
U_B_6_4	9.858	9.810	450.01	295.61	83.06	834.30	0.279
U_B_6_5	9.896	9.830	349.43	295.41	85.84	773.07	0.344
U_B_6_6	9.906	9.859	252.21	294.78	89.82	717.77	0.458
U_C_6_1	9.901	9.876	648.43	280.86	164.26	1139.73	0.201
U_C_6_2	9.842	9.800	202.09	280.37	164.19	650.66	0.471
U_D_6_1	9.892	9.834	650.23	256.29	287.19	1402.16	0.182
U_D_6_2	9.924	9.875	201.56	254.83	295.65	778.93	0.493
U_E_6_1	9.815	9.798	651.81	241.92	352.57	1546.68	0.172
U_E_6_2	9.824	9.842	201.63	242.49	350.27	771.33	0.442
U_E_6_2A	9.893	9.890	202.39	242.18	354.76	763.42	0.430
U_E_6_2B	9.850	9.827	202.15	242.53	351.23	818.81	0.483
U_E_6_3	9.881	9.893	549.31	242.48	352.80	1386.83	0.201
U_E_6_4	9.824	9.775	452.23	242.31	351.13	1234.86	0.240
U_E_6_5	9.858	9.801	351.92	242.49	351.75	1075.03	0.299
U_E_6_6	9.870	9.854	250.57	242.38	352.77	901.49	0.399
U_A_7_1	1.017	0.987	544.10	131.00	214.90	1284.13	0.181
U_A_7_2	1.012	0.956	497.14	129.50	220.26	1230.61	0.192
U_A_7_3	1.012	0.965	450.14	129.00	222.39	1157.24	0.203
U_A_7_4	0.990	0.942	402.12	129.92	214.19	1076.13	0.219
U_A_7_5	0.985	0.956	352.18	129.00	217.22	958.96	0.223
U_A_7_6	1.021	0.978	302.97	129.96	220.03	836.01	0.227
U_A_7_7	0.977	0.951	241.76	130.09	210.92	685.13	0.240
U_A_7_8	1.018	0.979	208.22	132.48	208.62	616.24	0.257
U_A_7_9	1.016	0.953	646.84	130.75	215.62	1486.73	0.173
U_B_7_1	1.018	0.956	647.01	161.08	85.70	1257.52	0.191
U_B_7_2	0.999	0.956	200.04	161.40	80.58	490.48	0.259
U_B_7_3	1.027	0.945	546.91	160.82	88.54	1170.03	0.218
U_B_7_4	1.004	0.963	448.35	160.91	83.65	1039.71	0.242
U_B_7_5	1.014	0.951	349.09	161.07	84.94	867.83	0.262
U_B_7_6	1.015	0.961	250.61	160.99	85.41	616.64	0.258
U_E_7_1	1.007	0.952	646.98	97.71	353.87	1696.95	0.144
U_E_7_2	1.016	0.973	203.23	97.66	355.84	694.81	0.241
U_E_7_3	1.005	0.957	548.92	97.60	353.91	1484.98	0.154
U_E_7_4	0.992	0.958	450.15	97.08	353.64	1282.68	0.172
U_E_7_5	0.998	0.957	349.15	97.11	354.71	1017.57	0.180
U_E_7_6	0.987	0.951	249.85	97.84	349.39	801.69	0.218
U_A_8_1	1.512	1.473	553.00	150.75	210.36	1334.25	0.196
U_A_8_2	1.539	1.495	505.39	150.32	215.98	1249.48	0.201
U_A_8_3	1.526	1.446	447.85	150.90	211.60	1151.92	0.216
U_A_8_4	1.548	1.491	399.63	151.45	212.34	1039.13	0.220
U_A_8_5	1.544	1.464	351.53	150.73	214.82	926.42	0.223
U_A_8_6	1.526	1.473	303.41	149.79	216.36	839.19	0.238
U_A_8_7	1.548	1.508	251.56	149.96	218.72	720.77	0.250
U_A_8_8	1.546	1.478	199.13	151.06	213.76	609.24	0.277
U_A_8_9	1.550	1.496	647.82	151.28	213.28	1512.69	0.185
U_A_9_1	0.553	0.477	543.76	103.35	223.23	1241.46	0.161
U_A_9_2	0.567	0.496	443.93	105.23	219.13	1129.81	0.193
U_A_9_3	0.563	0.513	344.03	104.72	220.33	985.42	0.230
U_A_9_4	0.565	0.506	295.47	105.68	216.97	870.40	0.241

Run No.	P_{in} (MPa)	P_{out} (MPa)	G (kg/m^2s)	T_{in} (oC)	Δh_i (kJ/kg)	q_c (kW/m^2)	X_c (–)
U_A_9_5	0.564	0.511	247.69	105.26	218.24	723.30	0.238
U_A_9_6	0.564	0.520	205.12	106.08	214.79	594.36	0.237
U_A_9_7	0.583	0.508	646.89	105.31	223.77	1378.44	0.143
U_A_9_8	0.566	0.504	499.43	105.63	217.46	1185.87	0.175
U_A_9_9	0.552	0.490	398.10	106.29	211.42	1040.25	0.206
U_B_9_1	0.598	0.518	648.76	137.50	91.33	1143.86	0.164
U_B_9_2	0.554	0.512	199.43	137.42	78.73	522.44	0.270
U_B_9_3	0.583	0.499	544.98	137.33	87.66	1064.98	0.188
U_B_9_4	0.565	0.494	447.65	137.33	82.37	1005.49	0.224
U_B_9_5	0.577	0.520	348.34	137.27	86.33	813.46	0.233
U_B_9_6	0.571	0.513	249.36	137.77	82.26	619.45	0.253
U_C_9_1	0.606	0.516	648.67	118.75	173.35	1282.63	0.150
U_C_9_2	0.564	0.519	200.78	119.36	158.59	571.92	0.259
U_D_9_1	0.594	0.522	643.78	89.42	293.88	1480.99	0.130
U_D_9_2	0.569	0.506	200.59	89.55	286.04	613.66	0.223
U_E_9_1	0.583	0.508	645.71	72.83	360.35	1525.07	0.106
U_E_9_2	0.540	0.508	200.83	72.29	349.71	623.65	0.197
U_E_9_3	0.564	0.508	545.23	72.68	355.36	1342.37	0.120
U_E_9_4	0.560	0.503	450.25	72.64	354.21	1205.35	0.145
U_E_9_5	0.547	0.494	352.20	72.31	351.80	996.29	0.164
U_E_9_6	0.540	0.498	249.28	72.30	349.85	712.62	0.168
U_A_10_1	3.064	2.982	549.10	187.51	216.58	1327.56	0.210
U_A_10_2	3.014	2.960	452.13	187.35	212.97	1129.55	0.223
U_A_10_3	3.008	3.011	351.29	187.95	209.79	939.67	0.249
U_A_10_4	2.948	2.884	299.39	187.00	208.74	864.46	0.278
U_A_10_5	2.980	2.960	253.67	187.78	204.37	791.08	0.312
U_A_10_6	2.961	2.935	197.77	187.11	209.46	658.36	0.338
U_A_10_7	3.101	3.036	650.16	188.09	217.21	1515.65	0.198
U_A_10_8	3.048	3.035	398.39	186.88	218.01	1034.62	0.234
U_A_10_9	3.059	2.973	502.61	188.23	212.96	1226.62	0.216
U_A_11_1	14.992	14.973	651.25	310.35	214.13	1127.38	0.209
U_A_11_2	15.033	14.982	547.95	311.04	211.86	1039.01	0.252
U_A_11_3	14.948	14.918	503.34	308.89	220.79	997.64	0.263
U_A_11_4	15.003	14.990	451.08	310.40	214.30	924.49	0.287
U_A_11_5	15.003	14.942	303.48	310.30	214.86	707.81	0.355
U_A_11_6	15.146	15.122	351.14	310.89	217.28	772.59	0.324
U_A_11_7	14.996	14.925	399.85	309.86	217.14	841.72	0.298
U_A_11_8	14.974	14.947	250.95	310.11	214.83	648.44	0.416
U_A_11_9	14.974	14.918	202.16	310.45	212.85	579.64	0.487
U_B_11_1	15.022	14.990	650.44	331.89	79.51	869.29	0.247
U_B_11_2	15.001	14.938	201.18	330.23	90.11	516.52	0.536
U_B_11_3	14.932	14.890	553.07	329.20	94.24	847.55	0.279
U_B_11_4	15.029	14.968	454.11	330.42	89.98	770.98	0.325
U_B_11_5	15.003	14.933	353.24	331.10	84.13	652.38	0.367
U_B_11_6	15.001	14.942	252.34	332.32	75.48	538.25	0.445
U_C_11_1	15.012	14.936	652.63	318.75	164.89	1027.10	0.220
U_C_11_2	14.981	14.960	201.84	319.39	159.71	538.16	0.490
U_D_11_1	15.012	14.938	650.25	296.92	289.97	1253.82	0.182
U_D_11_2	14.932	14.933	200.87	297.61	283.09	632.67	0.485

Run No.	P_{in} (MPa)	P_{out} (MPa)	G (kg/m^2s)	T_{in} (oC)	Δh_i (kJ/kg)	q_c (kW/m^2)	X_c (–)
U_E_11_1	15.051	15.006	652.89	284.72	355.97	1355.48	0.153
U_E_11_2	15.025	14.951	201.94	284.52	355.93	693.82	0.485
U_E_11_3	15.025	14.951	548.51	285.21	352.39	1251.99	0.207
U_E_11_4	14.979	14.929	448.97	284.96	351.82	1121.63	0.259
U_E_11_5	15.036	14.955	350.36	284.81	354.85	937.95	0.301
U_E_11_6	15.016	14.964	249.78	284.77	354.31	751.09	0.382
U_E_11_6A	15.022	14.960	249.93	285.11	352.81	756.70	0.388

Appendix B. CHF Data Base for Non-Uniformly Heated Vertical Annulus

Low-Flow CHF Data with Non-Uniformly Heated Vertical Annulus

1) Geometry

- Annulus inner diameter : 9.53 mm
- Annulus outer diameter : 19.4 mm
- Heated length : 1843 mm
- Axial heat flux profile : symmetric chopped cosine

2) Nomenclature

- P_{in} : Inlet pressure
- P_{out} : Outlet pressure
- G : Mass flux
- T_{in} : Inlet water temperature
- Δh_i : Inlet subcooling
- q_c : CHF (average heat flux for whole heated length)
- X_c : Exit quality
- L_C : CHF location from inlet
- Q_t : Total power delivered to the test section

Run No.	P_{in} (MPa)	P_{out} (MPa)	G (kg/m^2s)	T_{in} (°C)	Δh_i (kJ/kg)	q_c (kW/m^2)	Q_t (kW)	X_c (-)	L_C (m)
NU_A_1_1	1.829	1.789	200.89	160.32	210.67	604.211	33.431	0.277	1.646
NU_A_1_2	1.832	1.791	250.00	160.90	208.46	683.734	37.836	0.243	1.545
NU_A_1_3	1.837	1.793	348.62	160.19	212.14	905.042	50.076	0.223	1.545
NU_A_1_4	1.833	1.785	450.89	159.83	213.13	1130.092	62.528	0.211	1.545
NU_A_1_5	1.837	1.786	549.11	159.55	214.94	1316.465	72.839	0.196	1.545
NU_A_1_6A	1.838	1.782	647.32	160.52	210.56	1502.638	83.141	0.189	1.545
NU_B_1_1	1.826	1.788	200.89	188.53	86.60	503.271	27.846	0.277	1.646
NU_B_1_2	1.824	1.785	250.00	187.85	89.25	566.615	31.348	0.245	1.545
NU_B_1_3	1.831	1.789	352.68	188.18	88.68	761.554	42.133	0.232	1.545
NU_B_1_4	1.831	1.785	450.89	187.89	90.08	961.356	53.187	0.227	1.545
NU_B_1_5	1.845	1.794	549.12	189.67	83.80	1076.373	58.368	0.209	1.336
NU_B_1_5A	1.846	1.798	551.43	188.61	88.71	1055.002	58.568	0.200	1.545
NU_B_1_5B	1.826	1.775	552.08	188.50	86.73	1114.021	61.659	0.214	1.546
NU_B_1_6	1.848	1.792	649.55	189.07	86.87	1265.811	70.031	0.206	1.336
NU_B_1_6A	1.843	1.786	651.34	189.63	83.69	1257.768	69.586	0.205	1.646
NU_C_1_1	1.856	1.817	200.89	170.45	169.84	567.357	31.389	0.275	1.646
NU_C_1_2	1.827	1.773	651.74	171.07	163.60	1379.937	76.345	0.187	1.545
NU_D_1_1	1.813	1.773	200.12	143.54	280.96	652.686	36.116	0.272	1.646
NU_D_1_2	1.823	1.770	648.95	143.58	282.09	1623.271	89.821	0.174	1.545
NU_E_1_1	1.823	1.781	200.89	127.93	348.94	690.763	38.213	0.260	1.646
NU_E_1_2	1.823	1.780	250.00	127.09	352.44	821.276	45.433	0.238	1.646
NU_E_1_3	1.824	1.778	348.48	127.53	350.67	1074.926	59.469	0.213	1.646
NU_E_1_4	1.837	1.789	450.89	128.59	347.78	1294.650	71.624	0.188	1.646
NU_E_1_5	1.838	1.786	549.11	128.11	349.94	1548.016	85.644	0.180	1.646
NU_E_1_6	1.830	1.776	647.53	127.18	352.90	1785.097	98.874	0.170	1.545
NU_A_2_1	12.103	12.071	201.24	289.57	211.86	678.844	37.659	0.515	1.649
NU_A_2_2	12.105	12.072	250.78	289.83	210.63	754.239	41.841	0.441	1.649
NU_A_2_3	12.104	12.070	350.61	289.12	214.27	908.587	50.404	0.353	1.548
NU_A_2_4	12.122	12.086	450.72	289.44	213.29	1056.135	58.590	0.303	1.839
NU_A_2_5	12.109	12.072	550.68	289.74	211.14	1177.216	65.307	0.264	1.884
NU_A_2_6	12.116	12.078	649.39	289.69	211.75	1304.379	72.361	0.235	1.839
NU_A_2_4A	12.100	12.064	450.15	289.75	210.74	1029.184	57.156	0.293	1.839
NU_A_2_5A	12.067	12.030	548.86	290.26	211.75	1156.972	64.253	0.256	1.839
NU_A_2_6A	12.058	12.020	650.27	289.86	208.42	1291.600	71.730	0.233	1.548
NU_B_2_1	12.149	12.120	200.62	312.67	83.18	574.205	31.859	0.520	1.649
NU_B_2_2	12.121	12.091	250.31	313.98	74.02	643.180	35.686	0.466	1.649

Run No.	P_{in} (MPa)	P_{out} (MPa)	G (kg/m^2s)	T_{in} (^oC)	Δh_i (kJ/kg)	q_c (kW/m^2)	Q_t (kW)	X_c (–)	L_C (m)
NU_B_2_2A	12.218	12.188	250.38	312.37	87.92	611.735	33.941	0.431	1.649
NU_B_2_3	12.101	12.069	348.61	310.89	91.86	714.736	39.654	0.344	1.649
NU_B_2_4	12.214	12.181	451.21	312.61	86.25	814.953	45.216	0.301	1.599
NU_B_2_5	12.186	12.151	544.50	311.96	89.03	901.370	50.010	0.267	1.839
NU_B_2_6	12.144	12.108	651.50	311.27	91.42	997.614	55.349	0.239	1.839
NU_E_2_1	12.117	12.082	200.83	260.49	360.04	812.567	45.068	0.531	1.839
NU_E_2_1A	12.109	12.074	200.33	262.00	352.35	782.339	43.440	0.508	1.649
NU_E_2_2	12.119	12.084	251.08	261.47	355.35	883.377	48.997	0.426	1.649
NU_E_2_3	12.108	12.071	348.54	261.54	351.57	1127.444	62.535	0.370	1.839
NU_E_2_3A	12.101	12.065	351.56	262.26	350.77	1102.008	61.191	0.350	1.839
NU_E_2_4	12.110	12.073	451.51	262.16	351.63	1285.331	71.293	0.290	1.839
NU_E_2_4A	12.108	12.070	449.60	262.02	352.21	1260.477	69.990	0.281	1.839
NU_E_2_5	12.124	12.085	551.93	262.62	349.93	1468.452	81.451	0.253	1.839
NU_E_2_5A	12.124	12.085	550.24	262.07	352.75	1439.278	79.919	0.242	1.839
NU_E_2_6	12.112	12.072	649.94	261.48	355.04	1646.368	91.319	0.223	1.839
NU_E_2_6A	12.170	12.130	652.59	262.29	353.40	1592.411	88.422	0.205	1.839
NU_A_3_1	4.057	4.020	200.30	205.03	215.46	697.335	38.651	0.373	1.647
NU_A_3_2	4.078	4.041	249.91	205.82	216.43	815.881	45.222	0.342	1.647
NU_A_3_3	4.048	4.009	353.63	205.78	211.47	1002.945	55.590	0.283	1.647
NU_A_3_4	4.101	4.060	450.99	205.48	216.60	1191.525	66.043	0.253	1.546
NU_A_3_5	4.045	4.002	550.42	205.57	212.19	1341.086	74.333	0.225	1.546
NU_A_3_6	4.011	3.965	649.45	205.04	212.17	1509.414	83.663	0.209	1.546
NU_B_3_1	4.012	3.978	201.89	233.46	81.53	611.320	33.889	0.385	1.648
NU_B_3_2	4.088	4.052	249.90	233.75	86.13	677.539	37.560	0.339	1.648
NU_B_3_3	4.028	3.991	350.95	233.63	81.88	821.077	45.517	0.287	1.648
NU_B_3_4	4.016	3.976	450.86	233.22	82.97	977.632	54.196	0.262	1.547
NU_B_3_5	4.036	3.994	551.11	233.05	85.20	1102.483	61.118	0.237	1.547
NU_B_3_6	4.025	3.980	651.51	233.38	83.32	1203.625	66.724	0.216	1.547
NU_E_3_1	4.032	3.994	200.54	174.12	350.84	805.549	44.641	0.370	1.647
NU_E_3_2	4.022	3.983	251.02	173.54	352.65	939.750	52.078	0.330	1.647
NU_E_3_3	4.076	4.035	351.37	173.77	355.48	1197.253	66.349	0.281	1.647
NU_E_3_4	4.070	4.027	450.59	173.68	355.48	1425.195	78.982	0.246	1.546
NU_E_3_5	4.041	3.996	547.33	174.11	351.53	1629.379	90.297	0.221	1.546
NU_E_3_6	4.112	4.065	648.32	174.22	356.02	1830.633	101.451	0.197	1.546
NU_A_4_1	5.843	5.807	200.89	230.55	211.36	720.059	39.964	0.422	1.648
NU_A_4_2	5.843	5.807	252.38	230.44	211.93	833.773	46.275	0.378	1.648
NU_A_4_3	5.944	5.906	349.00	230.83	215.77	1016.267	56.404	0.317	1.648
NU_A_4_4	5.920	5.881	449.80	230.23	217.25	1178.052	65.382	0.270	1.648
NU_A_4_5	5.925	5.884	550.55	230.39	216.79	1341.531	74.456	0.242	1.547
NU_A_4_6	5.864	5.820	651.54	230.41	213.21	1487.276	82.545	0.219	1.547
NU_B_4_1	5.806	5.773	203.30	257.09	82.33	596.339	33.102	0.402	1.648
NU_B_4_1A	5.842	5.809	201.47	257.46	82.57	617.758	34.291	0.423	1.648
NU_B_4_2	5.863	5.829	251.77	256.45	88.72	719.892	39.960	0.388	1.648
NU_B_4_3	5.782	5.747	351.15	257.34	79.71	835.329	46.368	0.317	1.648
NU_B_4_4	5.749	5.712	452.10	257.11	78.93	965.511	53.095	0.280	1.547
NU_B_4_5	5.909	5.871	554.36	256.62	90.51	1055.044	58.564	0.238	1.547
NU_B_4_6B	5.764	5.723	648.80	257.23	79.24	1159.985	64.389	0.226	1.547
NU_B_4_6	5.989	5.948	650.12	257.40	91.20	1185.813	65.824	0.226	1.547
NU_C_4_1	5.903	5.868	200.52	240.35	168.68	696.293	38.647	0.433	1.648
NU_C_4_2	5.835	5.792	649.23	240.52	163.99	1359.009	75.431	0.221	1.547
NU_D_4_1	5.777	5.740	200.05	214.29	282.48	788.993	43.738	0.431	1.648
NU_D_4_2	5.841	5.797	650.12	213.36	290.32	1659.123	91.978	0.211	1.547
NU_E_4_1	5.859	5.822	198.89	200.06	351.32	848.501	47.035	0.439	1.648
NU_E_4_2	5.930	5.892	247.00	199.21	359.11	962.027	53.328	0.377	1.648
NU_E_4_3	5.751	5.711	350.28	199.46	347.80	1172.969	65.021	0.297	1.648
NU_E_4_4	5.776	5.735	445.67	199.69	348.27	1410.492	78.188	0.269	1.547

Run No.	P_{in} (MPa)	P_{out} (MPa)	G (kg/m^2s)	T_{in} (^oC)	Δh_i (kJ/kg)	q_c (kW/m^2)	Q_t (kW)	X_c (–)	L_C (m)
NU_E_4_5	5.767	5.724	547.40	199.84	347.08	1599.516	88.666	0.232	1.547
NU_E_4_6	5.923	5.879	651.07	199.90	355.62	1794.013	99.450	0.202	1.547
NU_A_5_1	8.000	7.965	201.61	253.13	216.22	720.510	39.999	0.457	1.648
NU_A_5_2	7.922	7.887	251.56	253.37	211.27	833.846	46.291	0.415	1.598
NU_A_5_3	8.004	7.967	350.82	253.28	215.67	994.306	55.199	0.332	1.648
NU_A_5_4	8.214	8.176	450.63	254.15	221.48	1125.911	62.505	0.273	1.547
NU_A_5_4A	7.951	7.913	450.23	253.10	214.00	1124.576	62.431	0.275	1.547
NU_A_5_5	7.986	7.946	550.06	253.88	211.89	1270.544	70.533	0.245	1.547
NU_A_5_6	7.960	7.919	650.04	254.00	210.08	1384.234	76.845	0.216	1.547
NU_B_5_1	8.087	8.055	202.04	279.30	89.02	640.781	35.578	0.479	1.649
NU_B_5_2	7.980	7.947	252.04	278.68	87.09	709.996	39.420	0.418	1.649
NU_B_5_3	7.975	7.941	350.36	278.57	87.38	824.446	45.775	0.339	1.649
NU_B_5_4	7.964	7.928	451.11	279.29	83.08	913.085	50.697	0.286	1.649
NU_B_5_5	7.952	7.914	549.79	278.68	85.67	1019.960	56.631	0.255	1.548
NU_B_5_6	7.920	7.881	649.24	279.35	80.61	1084.194	60.198	0.227	1.548
NU_E_5_1	7.993	7.957	201.56	223.69	354.52	840.597	46.657	0.463	1.648
NU_E_5_2	8.060	8.023	250.97	224.62	353.47	953.256	52.911	0.402	1.547
NU_E_5_3	8.104	8.066	350.47	225.05	353.58	1179.723	65.481	0.329	1.547
NU_E_5_4	8.030	7.991	451.46	224.42	352.95	1362.211	75.611	0.269	1.547
NU_E_5_5	8.064	8.022	552.06	223.98	356.56	1546.272	85.827	0.230	1.547
NU_E_5_6	7.971	7.928	648.04	223.89	352.55	1703.917	94.577	0.202	1.547
NU_E_5_6A	8.029	7.987	645.52	224.65	351.84	1677.568	93.113	0.198	1.547
NU_E_5_6B	8.023	7.980	651.58	224.31	353.11	1690.328	93.822	0.197	1.547
NU_A_6_1	9.873	9.840	204.32	271.67	210.17	671.155	37.266	0.448	1.649
NU_A_6_1A	9.907	9.874	200.29	271.22	213.97	741.155	41.152	0.523	1.649
NU_A_6_2	9.840	9.806	252.93	271.07	211.77	775.013	43.032	0.406	1.548
NU_A_6_3	9.844	9.809	354.52	271.77	208.43	926.310	51.433	0.325	1.548
NU_A_6_4	9.788	9.751	451.93	269.42	217.79	1075.086	59.693	0.274	1.548
NU_A_6_4A	9.746	9.709	451.46	271.68	204.57	1068.940	59.353	0.281	1.548
NU_A_6_5	9.863	9.825	548.12	272.16	207.24	1157.659	64.279	0.234	1.598
NU_A_6_5A	9.680	9.642	551.23	271.28	203.64	1182.398	65.652	0.240	1.548
NU_A_6_6	9.870	9.831	652.16	271.03	213.32	1281.308	71.144	0.202	1.548
NU_A_6_6A	9.875	9.836	654.59	271.17	212.82	1282.793	71.226	0.201	1.548
NU_B_6_1	9.985	9.954	201.02	295.58	88.86	619.031	34.376	0.504	1.649
NU_B_6_1A	9.911	9.881	201.74	294.95	89.11	585.306	32.504	0.469	1.649
NU_B_6_2	9.833	9.801	249.96	294.83	86.27	699.861	38.865	0.450	1.649
NU_B_6_3	9.843	9.810	349.63	296.14	79.42	794.663	44.130	0.359	1.649
NU_B_6_4	9.852	9.817	452.89	295.57	82.97	862.939	47.921	0.289	1.649
NU_B_6_5	9.885	9.849	551.04	295.45	85.16	931.440	51.726	0.248	1.649
NU_B_6_6	9.874	9.837	657.36	294.22	91.46	1015.751	56.407	0.216	1.548
NU_B_6_6A	9.894	9.856	648.77	295.73	83.95	1003.968	55.753	0.222	1.548
NU_C_6_1	9.902	9.870	199.69	281.09	163.12	707.459	39.284	0.531	1.649
NU_C_6_2	9.847	9.809	650.65	281.33	159.29	1171.447	65.048	0.213	1.548
NU_D_6_1	9.847	9.813	199.54	255.73	287.95	761.254	42.264	0.487	1.548
NU_D_6_2	9.883	9.842	647.01	255.62	290.01	1490.531	82.754	0.207	1.548
NU_E_6_1	9.863	9.827	202.46	241.91	354.71	794.448	44.104	0.457	1.648
NU_E_6_1A	9.837	9.802	201.00	241.96	353.38	800.866	44.460	0.469	1.648
NU_E_6_2	9.848	9.812	251.81	243.86	345.74	950.968	52.736	0.436	1.547
NU_E_6_3	9.852	9.815	349.77	242.68	350.63	1117.890	61.993	0.326	1.547
NU_E_6_4	9.863	9.825	452.48	243.09	349.17	1291.471	71.619	0.264	1.547
NU_E_6_4A	9.875	9.836	452.64	241.95	355.04	1294.048	71.840	0.260	1.648
NU_E_6_5	9.975	9.935	548.48	241.79	360.14	1527.380	84.701	0.244	1.547
NU_E_6_5A	9.897	9.857	547.42	242.14	355.08	1493.250	82.898	0.236	1.547
NU_E_6_6	9.868	9.827	652.28	243.71	346.41	1607.714	89.160	0.194	1.548
NU_E_6_6A	9.861	9.820	652.04	242.72	350.81	1609.557	89.260	0.191	1.547
NU_E_6_6B	9.853	9.811	650.79	242.85	349.84	1592.185	88.391	0.188	1.547

Run No.	P_{in} (MPa)	P_{out} (MPa)	G (kg/m^2s)	T_{in} (^oC)	Δh_i (kJ/kg)	q_c (kW/m^2)	Q_t (kW)	X_c (–)	L_C (m)
NU_A_7_1	1.005	0.964	198.60	131.42	210.64	588.118	30.877	0.256	1.646
NU_A_7_2	1.004	0.962	248.15	130.97	212.50	659.520	36.486	0.218	1.545
NU_A_7_3	1.009	0.963	348.28	131.13	212.68	861.337	47.702	0.196	1.336
NU_A_7_4	1.017	0.966	448.73	131.26	213.64	1058.897	58.644	0.182	1.336
NU_A_7_5	1.013	0.957	549.73	130.83	214.64	1222.952	67.728	0.165	1.336
NU_A_7_6	1.023	0.962	648.47	129.86	220.82	1398.363	77.362	0.153	1.336
NU_B_7_1	0.995	0.958	202.74	161.02	81.58	450.538	24.955	0.229	1.446
NU_B_7_2	1.000	0.961	251.23	160.48	84.85	545.475	30.214	0.223	1.336
NU_B_7_3	0.995	0.950	351.36	160.48	83.85	768.989	42.595	0.225	1.336
NU_B_7_4	1.009	0.958	450.86	160.71	85.58	936.440	51.870	0.211	1.336
NU_B_7_5	1.014	0.955	549.52	160.54	87.30	1117.245	61.885	0.205	1.336
NU_B_7_6	1.026	0.959	647.10	160.33	90.38	1263.651	69.994	0.194	1.646
NU_B_7_6A	1.028	0.961	647.19	160.99	87.99	1266.776	70.168	0.196	1.646
NU_E_7_1	0.993	0.951	200.06	98.17	349.24	650.094	35.958	0.223	1.646
NU_E_7_2	1.008	0.964	251.15	97.60	354.43	775.793	42.911	0.201	1.646
NU_E_7_3	1.021	0.974	347.68	98.26	354.15	1019.981	56.418	0.182	1.545
NU_E_7_4	1.023	0.973	451.00	98.07	355.45	1233.523	68.230	0.157	1.336
NU_E_7_5	1.018	0.964	550.52	97.82	355.42	1411.315	78.064	0.136	1.336
NU_E_7_6	1.013	0.956	650.01	98.47	351.77	1547.713	85.609	0.116	1.336
NU_A_8_1	1.533	1.494	200.55	151.21	211.31	609.189	33.745	0.276	1.646
NU_A_8_2	1.535	1.494	253.62	152.00	208.19	700.433	38.800	0.242	1.646
NU_A_8_3	1.541	1.498	350.47	151.03	213.27	919.421	50.930	0.222	1.646
NU_A_8_4	1.556	1.509	450.48	151.26	214.35	1119.267	62.001	0.204	1.545
NU_A_8_5	1.562	1.510	550.21	151.38	214.54	1326.879	73.502	0.195	1.646
NU_A_8_6	1.540	1.483	647.75	151.91	209.23	1467.327	81.282	0.179	1.545
NU_B_8_1	1.537	1.500	202.76	180.21	85.51	473.943	26.258	0.251	1.647
NU_B_8_2	1.537	1.499	253.63	180.05	86.21	538.815	29.852	0.224	1.647
NU_B_8_3	1.536	1.495	357.57	180.10	85.90	720.444	39.915	0.210	1.546
NU_B_8_3A	1.534	1.493	353.32	180.34	84.59	707.423	39.193	0.210	1.596
NU_B_8_4	1.527	1.480	446.44	180.59	82.46	941.460	52.160	0.224	1.337
NU_B_8_4A	1.542	1.497	451.49	181.05	82.61	933.537	51.721	0.219	1.337
NU_B_8_5	1.554	1.502	551.27	180.01	88.83	1134.458	62.852	0.215	1.546
NU_B_8_6	1.558	1.500	650.57	180.08	89.00	1258.263	69.712	0.199	1.647
NU_B_8_6A	1.564	1.506	651.59	179.85	90.89	1275.736	70.680	0.201	1.647
NU_E_8_1	1.557	1.515	200.39	118.47	354.43	682.824	37.817	0.249	1.646
NU_E_8_2	1.529	1.486	249.52	118.35	351.07	808.607	44.782	0.229	1.646
NU_E_8_3	1.559	1.514	345.98	118.03	356.58	1055.596	58.462	0.203	1.646
NU_E_8_3A	1.556	1.512	349.41	117.83	357.13	1071.741	59.356	0.204	1.646
NU_E_8_4	1.550	1.502	448.55	118.44	353.64	1297.311	71.848	0.184	1.545
NU_E_8_5	1.552	1.500	549.28	117.92	356.11	1550.837	85.888	0.174	1.545
NU_E_8_6	1.542	1.486	647.38	119.13	349.64	1765.387	97.773	0.165	1.545
NU_A_9_1	0.560	0.518	200.82	106.75	210.96	526.593	29.125	0.207	1.335
NU_A_9_2	0.560	0.515	250.06	106.93	210.05	617.372	34.146	0.189	1.335
NU_A_9_3	0.569	0.521	350.77	106.99	212.61	757.393	41.890	0.152	1.335
NU_A_9_4	0.569	0.515	447.91	107.25	211.58	926.793	51.259	0.142	1.645
NU_A_9_5	0.567	0.510	550.21	107.35	210.51	1008.299	55.767	0.114	1.105
NU_A_9_6	0.577	0.513	645.27	107.15	214.29	1166.293	64.505	0.110	1.335
NU_A_9_1A	0.553	0.511	200.60	106.90	208.12	524.702	29.020	0.207	1.335
NU_A_9_2A	0.561	0.517	249.53	107.10	209.67	632.923	35.006	0.197	1.335
NU_A_9_3A	0.563	0.513	349.47	106.91	211.09	800.003	44.247	0.168	1.335
NU_A_9_4A	0.568	0.512	449.00	106.29	215.07	967.775	53.526	0.150	1.335
NU_A_9_5A	0.576	0.515	547.97	107.01	214.50	1077.371	59.588	0.128	1.335
NU_A_9_6A	0.584	0.518	649.93	106.52	219.02	1265.670	70.002	0.124	1.335
NU_B_9_1	0.552	0.512	200.89	137.60	77.57	463.232	25.625	0.233	1.336
NU_B_9_2	0.565	0.522	249.43	137.50	81.77	560.225	30.990	0.224	1.336
NU_B_9_3	0.555	0.503	350.27	136.86	81.62	764.225	42.275	0.217	1.336

Run No.	P_{in} (MPa)	P_{out} (MPa)	G (kg/m^2s)	T_{in} (^oC)	Δh_i (kJ/kg)	q_c (kW/m^2)	Q_t (kW)	X_c (–)	L_C (m)
NU_B_9_4	0.565	0.501	449.35	136.77	84.96	984.230	54.445	0.216	1.336
NU_B_9_5	0.584	0.510	549.77	137.30	88.05	1103.586	61.048	0.194	1.336
NU_B_9_6	0.599	0.515	650.93	137.49	91.65	1210.112	66.941	0.175	1.646
NU_B_9_1A	0.544	0.504	199.00	137.05	77.34	478.558	26.473	0.245	1.336
NU_B_9_2A	0.545	0.501	249.29	137.27	76.69	568.115	31.427	0.230	1.336
NU_B_9_3A	0.546	0.494	348.11	137.12	77.65	765.389	42.339	0.220	1.106
NU_B_9_4A	0.569	0.506	449.46	136.77	85.92	941.724	52.094	0.205	1.336
NU_B_9_5A	0.573	0.502	549.91	137.19	85.32	1117.288	61.806	0.198	1.106
NU_B_9_6A	0.588	0.503	646.80	137.36	89.05	1209.366	66.899	0.177	1.646
NU_C_9_1	0.564	0.523	200.39	119.35	158.91	513.717	28.415	0.225	1.336
NU_C_9_2	0.588	0.515	644.49	119.50	165.08	1210.569	66.964	0.142	1.336
NU_C_9_1A	0.549	0.507	200.41	118.32	158.59	508.895	28.148	0.222	1.545
NU_C_9_2A	0.591	0.516	651.51	118.84	168.64	1256.270	69.371	0.146	1.336
NU_D_9_1	0.556	0.513	200.93	89.08	284.21	559.232	30.926	0.190	1.544
NU_D_9_2	0.576	0.518	651.51	90.22	285.38	1219.087	67.418	0.083	1.335
NU_D_9_1A	0.555	0.512	200.73	89.83	280.70	573.983	31.742	0.201	1.544
NU_D_9_2A	0.573	0.514	647.10	88.62	291.24	1225.845	67.791	0.083	1.335
NU_E_9_1	0.559	0.515	201.98	73.88	348.74	597.966	33.066	0.181	1.544
NU_E_9_2	0.563	0.518	249.56	73.49	351.71	676.848	37.427	0.151	1.335
NU_E_9_3	0.563	0.515	350.46	73.58	351.20	814.864	45.059	0.105	1.335
NU_E_9_4	0.570	0.520	450.70	73.51	353.73	997.410	55.154	0.091	1.335
NU_E_9_5	0.567	0.515	547.27	73.36	353.46	1113.151	61.554	0.070	1.335
NU_E_9_6	0.575	0.518	650.92	73.70	354.25	1310.583	72.471	0.067	1.335
NU_E_9_1A	0.559	0.516	200.15	73.13	352.08	613.820	33.942	0.192	1.335
NU_E_9_2A	0.559	0.514	250.27	73.84	349.13	717.982	39.702	0.170	1.335
NU_E_9_3A	0.563	0.514	349.57	73.70	350.62	885.298	48.954	0.130	1.335
NU_E_9_4A	0.569	0.518	449.84	73.50	353.38	1012.173	55.970	0.095	1.335
NU_E_9_5A	0.572	0.517	550.35	73.40	354.63	1190.241	65.816	0.085	1.335
NU_E_9_6A	0.571	0.511	650.93	73.92	352.18	1384.624	76.565	0.082	1.335
NU_A_10_1	3.023	2.985	199.59	187.11	214.81	671.569	37.216	0.340	1.647
NU_A_10_2	3.012	2.974	250.61	186.97	214.54	772.805	42.826	0.302	1.647
NU_A_10_3	3.031	2.991	350.08	187.61	213.34	976.452	54.112	0.263	1.647
NU_A_10_4	3.154	3.111	450.93	187.90	222.48	1166.976	64.670	0.231	1.647
NU_A_10_5	3.022	2.977	547.93	187.59	212.65	1336.245	74.050	0.215	1.546
NU_A_10_6	3.053	3.005	652.14	187.19	217.07	1504.337	83.365	0.195	1.546
NU_B_10_1	3.020	2.985	201.60	215.80	85.52	560.938	31.090	0.333	1.647
NU_B_10_2	3.021	2.985	252.48	215.75	85.87	662.560	36.722	0.311	1.647
NU_B_10_3	3.058	3.019	349.13	215.40	90.66	819.358	45.413	0.271	1.647
NU_B_10_4	3.009	2.968	451.69	215.82	84.50	950.689	52.692	0.241	1.647
NU_B_10_5	3.026	2.982	550.11	215.95	85.39	1089.535	60.388	0.223	1.647
NU_B_10_6	3.016	2.969	652.76	215.82	85.08	1219.560	67.595	0.208	1.647
NU_E_10_1	3.064	3.024	200.41	155.47	356.54	785.238	43.507	0.338	1.647
NU_E_10_2	3.050	3.009	250.13	155.85	353.72	905.276	50.158	0.299	1.647
NU_E_10_3	3.017	2.975	351.31	155.56	352.15	1159.167	64.225	0.255	1.546
NU_E_10_4	3.039	2.995	449.74	155.26	355.34	1379.595	76.438	0.222	1.647
NU_E_10_5	3.075	3.028	553.49	154.55	361.50	1615.979	89.534	0.199	1.647
NU_E_10_6	3.048	2.999	648.47	155.80	353.79	1852.857	101.164	0.194	1.546
NU_A_11_1	14.920	14.890	203.39	311.93	202.01	565.639	31.386	0.474	1.649
NU_A_11_1A	15.123	15.092	201.84	311.14	214.90	573.777	31.837	0.482	1.649
NU_A_11_1B	14.888	14.857	201.34	309.59	214.34	631.416	35.073	0.546	1.649
NU_A_11_2	15.011	14.980	249.74	311.46	208.08	718.621	39.874	0.494	1.650
NU_A_11_3	14.970	14.937	352.91	311.33	207.56	848.042	47.056	0.378	1.650
NU_A_11_4	15.042	15.008	453.85	309.91	218.73	947.657	52.584	0.291	1.840
NU_A_11_5	14.925	14.891	551.78	310.69	210.05	1059.359	58.782	0.257	1.840
NU_A_11_5A	15.055	15.020	554.46	310.04	218.45	1059.514	58.790	0.249	1.840
NU_A_11_6	15.038	15.001	650.84	310.80	213.42	1199.793	66.575	0.237	1.650

Run No.	P_{in} (MPa)	P_{out} (MPa)	G (kg/m^2s)	T_{in} (^oC)	Δh_i (kJ/kg)	q_c (kW/m^2)	Q_t (kW)	X_c (–)	L_C (m)
NU_B_11_1	15.012	14.984	202.28	330.34	89.81	520.813	28.902	0.538	1.840
NU_B_11_2	15.026	14.997	253.77	331.01	85.77	583.413	32.375	0.475	1.840
NU_B_11_3	15.016	14.986	350.03	331.62	81.09	680.084	37.740	0.393	1.840
NU_B_11_4	15.049	15.018	449.48	331.31	84.67	765.655	42.489	0.332	1.840
NU_B_11_5	15.056	15.024	559.18	330.27	92.16	859.844	47.719	0.284	1.650
NU_B_11_5A	15.026	14.993	556.85	330.09	91.14	849.016	47.115	0.281	1.650
NU_B_11_5B	15.008	14.976	548.63	331.19	83.75	853.932	47.388	0.296	1.650
NU_B_11_6	15.107	15.073	649.81	330.34	93.85	948.130	52.616	0.264	1.549
NU_C_11_1	15.016	14.986	199.88	319.26	161.93	572.129	31.747	0.536	1.650
NU_C_11_2	14.988	14.953	656.43	318.90	163.00	1077.294	59.780	0.237	1.650
NU_D_11_1	15.021	14.989	202.37	297.45	287.50	669.858	37.165	0.522	1.649
NU_D_11_2	15.003	14.966	651.98	295.97	294.77	1353.033	75.072	0.220	1.677
NU_E_11_1	15.000	14.967	200.84	285.87	347.97	744.757	41.318	0.558	1.649
NU_E_11_2	15.001	14.967	251.37	285.39	350.50	846.438	46.960	0.472	1.649
NU_E_11_3	15.004	14.968	351.31	284.39	355.78	1032.354	57.274	0.362	1.649
NU_E_11_4	14.996	14.959	448.15	284.64	354.17	1198.358	66.484	0.299	1.649
NU_E_11_5	14.975	14.938	549.92	285.21	350.39	1350.183	74.908	0.249	1.649
NU_E_11_6	14.946	14.908	650.14	285.25	349.03	1469.070	81.504	0.203	1.839
NU_A_12_1	10.978	10.945	201.67	280.06	214.82	705.644	39.184	0.509	1.649
NU_A_12_2	10.975	10.942	250.70	280.69	211.43	776.651	43.127	0.434	1.649
NU_A_12_3	10.994	10.959	352.45	280.30	214.27	923.139	51.261	0.339	1.649
NU_A_12_4	10.983	10.947	449.23	280.95	210.46	1041.089	57.811	0.283	1.649
NU_A_12_5	10.997	10.959	548.41	281.41	208.61	1147.499	63.721	0.241	1.548
NU_A_12_6	11.034	10.996	650.26	281.69	208.73	1238.388	68.768	0.205	1.839
NU_A_13_1	13.469	13.438	200.95	299.08	216.08	664.491	36.906	0.537	1.649
NU_A_13_2	13.548	13.516	249.77	299.41	217.42	751.535	41.741	0.472	1.839
NU_A_13_3	13.452	13.418	352.52	299.63	212.29	912.724	50.693	0.381	1.839
NU_A_13_4	13.461	13.426	451.72	301.85	200.36	1033.319	57.392	0.325	1.839
NU_A_13_5	13.489	13.453	551.87	300.80	207.32	1165.119	64.712	0.280	1.649
NU_A_13_6	13.478	13.441	653.31	301.37	203.71	1240.866	68.919	0.237	1.839

Appendix C. CHF Data Base for Zero-Flow Conditions

Zero-Flow CHF Data Base

1. Zero-Flow CHF Data with Uniformly Heated Vertical Annulus

1) Geometry

- Annulus inner diameter : 9.54 mm
- Annulus outer diameter : 19.4 mm
- Heated length : 1842 mm
- Axial heat flux profile : uniform

2) Nomenclature

P_{in} : Inlet pressure
P_{out} : Outlet pressure
Δh_i : Inlet subcooling
Q_t : Total power
$q_{c,\,avg}$: Average heat flux (CHF) for the whole heated length
L_{CHF} : CHF location from test section inlet

3) CHF data base

Run No.	P_{in} (MPa)	P_{out} (MPa)	Δh_i (kJ/kg)	Q_t (kW)	$q_{c,\,avg}$ (kW/m^2)	L_{CHF} (m)
A_1_P	1.814	1.787	238.853	16.640	301.42	1.835
B_1_P	1.791	1.785	85.221	15.321	277.52	1.836
B_1_PA	1.790	1.781	104.237	14.675	265.82	1.836
C_1_P	1.828	1.790	186.320	15.977	289.41	1.835
D_1_P	1.825	1.764	310.575	17.726	321.09	1.815
E_1_P	1.807	1.789	396.966	18.175	329.22	1.815
A_3_P	4.075	4.022	248.133	17.849	323.32	1.836
B_3_PA	4.033	3.990	137.820	16.198	293.41	1.816
C_3_P	4.074	4.019	178.808	16.970	307.39	1.836
D_3_P	4.030	3.976	330.034	19.174	347.32	1.836
E_3_P	4.009	4.005	413.302	19.725	357.30	1.836
A_4_P	5.874	5.828	225.367	17.292	313.23	1.837
A_4_PA	5.874	5.808	280.284	17.182	311.23	1.817
B_4_P	5.832	5.825	134.596	16.750	303.41	1.837
B_4_PA	5.861	5.836	124.667	17.617	319.11	1.837
C_4_P	5.813	5.836	178.759	17.513	317.23	1.837
D_4_P	5.861	5.844	302.910	17.845	323.24	1.837
E_4_P	5.881	5.783	367.986	18.610	337.10	1.836
A_6_P	9.851	9.826	238.029	15.320	277.51	1.838
A_6_PA	9.837	9.833	245.850	16.199	293.43	1.818
B_6_P	9.848	9.861	113.970	14.444	261.64	1.838
C_6_9	9.920	9.893	188.089	15.540	281.49	1.838
D_6_P	9.856	9.822	297.973	16.317	295.56	1.837
E_6_P	9.868	9.839	372.135	17.195	311.47	1.837
A_7_P	1.005	0.964	234.468	15.104	273.59	1.815
B_7_P	1.015	0.975	104.925	14.337	259.70	1.815
C_7_P	1.005	0.969	173.467	14.668	265.69	1.835

Run No.	P_{in} (MPa)	P_{out} (MPa)	Δh_i (kJ/kg)	Q_t (kW)	$q_{c,\,avg}$ (kW/m^2)	L_{CHF} (m)
D_7_P	1.016	0.967	296.490	14.561	263.76	1.835
E_7_P	1.005	0.959	336.110	14.787	267.85	1.834
A_9_P	0.566	0.516	203.117	12.255	221.99	1.834
B_9_P	0.567	0.523	123.442	12.265	222.17	1.834
C_9_P	0.556	0.525	185.516	12.384	224.32	1.834
D_9_P	0.566	0.516	286.090	13.451	243.65	1.834
E_9_P	0.568	0.523	370.776	14.454	261.82	1.834
A_11_P	15.016	14.947	262.635	12.484	226.13	1.838
B_11_P	14.996	14.990	225.285	12.238	221.68	1.838
C_1_P	14.972	14.982	151.768	11.143	201.84	1.738
D_11_P	15.014	14.986	337.756	12.595	228.14	1.838
E_11_P	14.981	14.990	378.422	13.167	238.51	1.838
E_11_PA	15.031	14.951	380.179	13.471	244.01	1.818
E_11_PB	15.007	14.960	373.256	17.408	315.33	1.838

2. Zero-Flow CHF Data with Non-Uniformly Heated Vertical Annulus

1) Geometry

- Annulus inner diameter : 9.53 mm
- Annulus outer diameter : 19.4 mm
- Heated length : 1843 mm
- Axial heat flux profile : symmetric chopped cosine

2) Nomenclature

P_{in} : Inlet pressure

P_{out} : Outlet pressure

Δh_i : Inlet subcooling

Q_t : Total power

$q_{c,\,avg}$: Average heat flux (CHF) for the whole heated length

L_{CHF} : CHF location from test section inlet

3) CHF data base

Run No.	P_{in} (MPa)	P_{out} (MPa)	Δh_i (kJ/kg)	Q_t (kW)	$q_{c,\,avg}$ (kW/m^2)	L_{CHF} (m)
NU_A_1_P	1.818	1.784	217.883	18.926	343.00	1.646
NU_B_1_P	1.825	1.794	91.805	17.153	310.87	1.596
NU_C_1_P	1.834	1.799	171.721	18.099	328.01	1.647
NU_D_1_P	1.829	1.793	289.792	19.519	353.74	1.646
NU_E_1_P	1.828	1.792	351.766	20.718	375.47	1.646
NU_A_2_P	12.127	12.099	222.112	19.628	355.72	1.839
NU_B_2_P	12.219	12.189	105.183	16.620	301.21	1.839
NU_C_2_P	12.010	11.978	170.132	18.265	331.02	1.839
NU_D_2_P	12.089	12.059	290.793	17.729	321.30	1.839
NU_D_2_PA	12.098	12.066	290.120	20.895	378.68	1.839
NU_E_2_P	12.095	12.065	353.919	23.858	432.38	1.649
NU_E_2_PA	12.160	12.129	351.296	22.650	410.49	1.649
NU_A_3_P	4.024	3.988	222.738	23.061	417.94	1.647
NU_B_3_P	4.026	3.992	89.149	20.344	368.70	1.648
NU_C_3_P	4.053	4.018	178.464	21.878	396.50	1.648
NU_D_3_P	4.083	4.048	297.761	24.066	436.15	1.647
NU_E_3_P	4.048	4.012	354.657	24.508	444.16	1.647
NU_A_3_PA	4.053	4.018	226.249	21.454	388.81	1.647
NU_A_3_PB	4.023	3.990	223.385	22.326	404.62	1.647
NU_D_3_PA	4.041	4.005	302.610	22.983	416.52	1.647
NU_D_3_PB	4.021	3.985	298.067	23.545	426.71	1.647
NU_E_3_PA	4.044	4.006	370.222	22.983	416.52	1.647
NU_E_3_PB	4.041	4.006	361.517	24.960	452.35	1.647
NU_A_3_PC	4.087	4.053	225.486	21.546	390.48	1.647
NU_B_3_PA	3.979	3.947	92.016	18.267	331.05	1.647
NU_C_3_PA	4.075	4.040	175.333	20.131	364.84	1.647
NU_D_3_PC	3.998	3.963	284.967	22.216	402.62	1.647

Run No.	P_{in} (MPa)	P_{out} (MPa)	Δh_i (kJ/kg)	Q_t (kW)	$q_{c,\,avg}$ (kW/m^2)	L_{CHF} (m)
NU_E_3_PC	4.043	4.008	343.816	22.316	404.43	1.647
NU_E_3_PD	4.067	4.032	355.960	23.530	426.44	1.647
NU_A_4_P	5.882	5.847	223.283	21.113	382.63	1.648
NU_A_4_PA	5.803	5.769	219.780	20.668	374.57	1.648
NU_B_4_P	5.860	5.828	86.568	18.695	338.81	1.648
NU_B_4_PA	5.810	5.776	116.903	19.767	358.24	1.648
NU_C_4_P	5.869	5.835	175.925	19.919	360.99	1.648
NU_C_4_PA	6.156	6.120	187.421	19.239	348.67	1.648
NU_D_4_P	5.882	5.845	293.272	22.976	416.40	1.648
NU_D_4_PA	5.898	5.861	292.706	21.663	392.60	1.648
NU_E_4_P	5.853	5.816	352.176	25.056	454.09	1.648
NU_E_4_PA	5.857	5.822	352.269	22.408	406.10	1.648
NU_E_4_PB	6.185	6.148	373.448	22.349	405.03	1.648
NU_A_5_P	8.030	7.997	234.857	20.557	372.56	1.648
NU_B_5_P	7.950	7.920	98.909	17.608	319.11	1.839
NU_C_5_P	7.936	7.905	183.191	19.026	344.81	1.836
NU_D_5_P	7.985	7.948	287.876	20.461	370.82	1.648
NU_D_5_PA	7.981	7.946	295.125	21.436	388.49	1.648
NU_D_5_PB	7.893	7.860	293.970	21.398	387.80	1.648
NU_E_5_P	7.985	7.949	357.546	24.204	438.65	1.648
NU_E_5_PA	7.945	7.909	352.870	23.385	423.81	1.648
NU_A_6_P	9.939	9.902	219.608	17.005	308.18	1.839
NU_B_6_P	9.847	9.814	94.133	18.588	336.87	1.649
NU_C_6_P	9.861	9.826	158.436	15.515	281.18	1.649
NU_D_6_P	9.866	9.824	295.906	18.806	340.82	1.838
NU_E_6_P	9.870	9.835	353.645	20.620	373.70	1.838
NU_A_6_PA	9.708	9.676	232.858	20.876	378.34	1.649
NU_B_6_PA	9.847	9.819	96.086	16.427	297.71	1.839
NU_C_6_PA	9.509	9.478	176.721	21.527	390.14	1.649
NU_C_6_PB	9.855	9.824	178.017	22.202	402.37	1.649
NU_D_6_PA	9.904	9.871	300.826	20.572	372.83	1.839
NU_E_6_PA	9.870	9.835	361.386	22.189	402.13	1.648
NU_E_6_PB	9.856	9.855	353.627	24.094	436.66	1.648
NU_A_6_PB	9.877	9.848	215.582	18.170	329.30	1.839
NU_B_6_PB	9.878	9.851	84.003	15.314	277.54	1.649
NU_C_6_PC	9.860	9.831	152.073	16.545	299.85	1.839
NU_D_6_PB	9.939	9.908	295.631	20.702	375.18	1.839
NU_E_6_PC	9.865	9.831	341.027	22.547	408.62	1.648
NU_A_7_P	1.008	0.974	221.714	16.633	301.44	1.646
NU_B_7_P	1.006	0.971	92.948	14.973	271.36	1.646
NU_C_7_P	1.004	0.970	179.792	16.351	296.33	1.646
NU_D_7_P	1.004	0.969	293.309	17.515	317.43	1.646
NU_E_7_P	1.006	0.972	353.894	18.499	335.26	1.646

Run No.	P_{in} (MPa)	P_{out} (MPa)	Δh_i (kJ/kg)	Q_t (kW)	$q_{c,\,avg}$ (kW/m^2)	L_{CHF} (m)
NU_A_8_P	1.526	1.491	219.129	18.095	327.94	1.646
NU_B_8_P	1.507	1.476	85.026	16.315	295.68	1.647
NU_C_8_P	1.520	1.485	162.903	16.863	305.61	1.646
NU_C_8_PA	1.538	1.505	188.199	17.945	325.22	1.646
NU_D_8_P	1.527	1.490	290.161	19.382	351.26	1.646
NU_E_8_P	1.526	1.489	347.937	20.336	368.55	1.646
NU_A_9_P	0.548	0.515	214.445	14.977	271.43	1.645
NU_B_9_PA	0.536	0.505	78.729	13.149	238.30	1.646
NU_C_9_P	0.555	0.521	156.639	14.447	261.82	1.646
NU_D_9_P	0.559	0.525	272.091	15.846	287.18	1.645
NU_E_9_P	0.547	0.510	353.766	17.073	309.42	1.594
NU_A_10_P	3.050	3.015	221.106	19.998	362.43	1.647
NU_A_10_PA	2.995	2.965	227.314	20.689	374.95	1.647
NU_B_10_P	3.028	2.997	94.639	18.341	332.40	1.647
NU_B_10_PA	3.006	2.973	99.960	18.750	339.81	1.647
NU_C_10_P	3.041	3.007	171.543	19.139	346.86	1.647
NU_D_10_P	3.025	2.990	290.063	21.094	382.29	1.647
NU_E_10_P	3.024	2.989	355.119	21.572	390.95	1.647
NU_E_10_PA	3.000	2.965	359.701	21.813	395.32	1.647
NU_D_11_P	14.966	14.941	288.053	12.360	224.00	1.649
NU_D_11_PA	14.954	14.927	287.919	15.416	279.39	1.839
NU_E_11_P	15.029	15.001	338.223	12.465	225.90	1.649
NU_E_11_PA	14.956	14.926	359.948	15.745	285.35	1.838
NU_E_11_PB	14.959	14.929	326.349	14.544	263.58	1.839

BIBLIOGRAPHIC INFORMATION SHEET

Performing Org. Report No.	Sponsoring Org. Report No.	Standard Report No.	INIS Subject Code
KAERI/TR-1919/2001			

Title / Subtitle	Experimental Study on the CHF in Uniformly and Non-Uniformly Heated Vertical Annuli
Project Manager and Department (or Main Author)	Se-Young Chun (Thermal Hydraulic Safety Research Team)
Researcher and Department	Se-Young Chun, Sang-Ki Moon, Heung-June Chung, Jong-Kuk Park, Bok-Deuk Kim, Young-Jung Youn, Moon-Ki Chung (Thermal Hydraulic Safety Research Team)

Publication Place	Taejon	Publisher	KAERI	Publication Date	2001
Page	98 p.	Ill. & Tab.	Yes(∨), No ( )	Size	26 Cm.
Note					
Classified	Open(∨), Restricted( ), ___ Class Document		Report Type	Technical Report	
Sponsoring Org.			Contract No.		

Abstract (15-20 Lines)

Up to now, KAERI has performed critical heat flux experiments in water under zero-flow and low-flow conditions using a RCS CHF loop facility with uniformly and non-uniformly heated vertical annulus. Since the existing CHF experiments were mainly performed under low-pressure conditions, we performed the CHF experiment to investigate the pressure effect on the CHF under zero-flow and low-flow conditions for a wide range of system pressures. Also, two vertical annuli with the same geometry have been used to investigate the axial heat flux distributions on the CHF. This report summarizes the experimental results and provides the CHF data that can be used for the development for CHF correlation and a thermal hydraulic analysis code.

The CHF data have been collected for system pressures ranging from 0.57 to 15.15 MPa, mass flux 0 and from 200 to 650 kg/m^{2}s, inlet subcooling from 75 to 360 kJ/kg and exit quality from 0.07 to 0.57. At low-flow conditions, the total number of data are 242 and 290 with uniformly heated- and non-uniformly heated test sections, respectively. 41 and 94 CHF data are generated with uniformly heated- and non-uniformly heated test sections, respectively, in zero-flow CHF experiments that are performed by blocking test section bottoms. The CHF experiment result shows that the effects of system pressure, mass flux and inlet subcooling are consistent with conventional understandings and similar to those for round tubes. The behavior of the CHF is relatively complex at low pressures. Also, the effects of axial heat flux profile are large at low-pressure conditions.

Subject Keywords (About 10 words)	Critical Heat Flux, Vertical Annulus, Uniformly and Non-Uniformly Heated, Low-Flow, Zero-Flow, Pressure Effect, CHF Data Base

서 지 정 보 양 식

수행기관보고서번호	위탁기관보고서번호	표준보고서번호	INIS 주제코드
KAERI/TR-1919/2001			

제목 / 부제	균일 및 비균일 가열 수직환상관에서 임계열유속에 대한 실험 연구
연구책임자 및 부서명 (AR,TR 등의 경우 주저자)	천세영 (열수력안전연구팀)
연 구 자 및 부 서 명	천세영, 문상기, 정흥준, 박종국, 김복득, 윤영중, 정문기 (열수력안전연구팀)

출 판 지	대전	발행기관	한국원자력연구소	발행년	2001
페 이 지	98 p.	도 표	있음(∨), 없음( )	크 기	26 cm
참고사항	원전 안전계통 실증실험				
비밀여부	공개(∨), 대외비( ), __ 급비밀		보고서종류	기술보고서	
연구위탁기관			계약번호		

초록 (15-20줄내외)

현재까지 한국원자력연구소에서는 RCS CHF Loop를 이용하여 Zero-Flow 및 저유속 조건에서 균일 및 비균일하게 가열되는 수직 환상관에서 물을 이용한 임계열유속 실험을 수행하였다. 저유속 조건에서 수행된 기존의 임계열유속 실험이 낮은 압력조건에서 주로 수행되었기 때문에, 본 실험에서는 광범위한 압력조건하에서 Zero-Flow 및 저유속 조건에서의 압력이 임계열유속에 미치는 영향을 살펴보았다. 또한 저유속 조건에서 수직방향 열유속분포가 미치는 영향을 고찰하기 위해, 동일한 기하학적 형상을 갖는 균일 및 비균일 가열 수직환상관을 이용하였다. 본 보고서는 이러한 일련의 실험들의 결과를 종합하고, 임계열유속 상관식의 개발 및 코드 개발에 이용될 수 있도록 임계열유속 실험 데이터를 제공하기 위해 작성되었다. 임계열유속 실험은 계통압력 0.54 - 15.15 MPa, 질량유속 0, 200 - 650 kg/m^{2}s, 입구과냉도 75 - 360 kJ/kg 및 출구건도 0.07 - 0.57의 조건에서 수행되었다. 저유속 조건에서는 균일 및 비균일하게 가열되는 수직환상관에서 각각 242개와 290개의 임계열유속 데이터를 생산하였다. 시험관 하부를 폐쇄하여 수행한 Zero-Flow 조건에서의 임계열유속 데이터는 균일 및 비균일 가열 시험관에서 각각 41개와 94개의 데이터가 생산되었다. 임계열유속 실험결과 임계열유속에 미치는 압력, 유량, 입구과냉도 등의 영향은 기존 원형관에서와 비슷하게 나타났다. 낮은 압력에서는 임계열유속의 거동이 복잡하게 나타났다. 또한 낮은 압력조건에서 수직방향 열유속분포가 임계열유속에 미치는 영향이 상대적으로 큰 것으로 나타났다.

주제명키워드 (10단어내외)	임계열유속, 수직환상관, 균일 및 비균일 가열, 저유량, Zero-Flow, 광범위한 압력조건, 임계열유속 데이터 베이스,